High-Temperature Materials

SCIEPublish

Review

Review on High-Temperature Porous Media Materials for Clean Combustion of Hydrogen and Ammonia Fuels

Cheng Ma [1,2,3], Liping Pan [1,2,3,*], Enjie Wang [1,2,3], Congjie Liu [1,2,3], Yawei Li [1,2,3,*], Xiong Liang [1,2,3], Yajie Dai [1,2,3] and Pengxiang Zhao [1,2,3]

[1] State Key Laboratory of Advanced Refractories, Wuhan University of Science and Technology, Wuhan 430081, China; macheng@wust.edu.cn (C.M.); 202427704301@wust.edu.cn (E.W.); lcj031104@wust.edu.cn (C.L.); liangxiong@wust.edu.cn (X.L.); yajie.dai@wust.edu.cn (Y.D.); pengxiang.zhao@wust.edu.cn (P.Z.)

[2] Joint International Research Laboratory of Refractories and Metallurgy, Wuhan University of Science and Technology, Wuhan 430081, China

[3] National-Provincial Joint Engineering Research Center of High Temperature Materials and Lining Technology, Wuhan University of Science and Technology, Wuhan 430081, China

* Corresponding author. E-mail: panliping@wust.edu.cn (L.P.); liyawei@wust.edu.cn (Y.L.)

Received: 1 September 2026; Revised: 17 September 2026; Accepted: 22 October 2026; Available online: 9 November 2026

ABSTRACT: Porous media combustion technology is regarded as one of the promising routes for efficient thermochemical conversion of hydrogen and ammonia fuels. However, porous skeletal materials are exposed to demanding service conditions including temperatures of 900–1500 °C, high-concentration water-vapor atmospheres, and frequent cyclic thermal shock, which can promote sintering, hydrothermal corrosion, oxidation, and thermomechanical fatigue cracking. Reviews addressing high-temperature material degradation, topological thermomechanical failure, manufacturing-induced defects and surface protection remain comparatively limited in the literature surveyed. In this work, four categories of high-temperature porous materials, *i.e.*, oxide ceramics, non-oxide ceramics, silicate refractories and intermetallic compounds, are comprehensively reviewed. The thermomechanical failure mechanisms of conventional disordered structures and novel additively-manufactured ordered topologies (including triply periodic minimal surfaces, TPMS) under cyclic thermal shock are discussed based on thermal-shock-resistance figure-of-merit R. High-temperature micro-defects originating from replica impregnation, extrusion, and lithography-based ceramic manufacturing (LCM) additive manufacturing are analyzed. Special attention is paid to the hydrothermal-volatilization corrosion mechanism of SiC in water-vapor-rich atmosphere generated by ammonia combustion, together with the performance of multi-layer protective coatings including mullite, cordierite, Al_2O_3–Cr_2O_3 solid-solution and rare-earth silicate systems. A synergistic fuel-material-topology-coating selection matrix is proposed for hydrogen, ammonia and blended fuels. Finally, key bottlenecks and future research directions, covering composite ultra-refractory ceramics, self-healing environmental barrier coatings, high-temperature additive manufacturing, and catalytic-refractory integrated porous architectures, are put forward. This review aims to provide material-oriented references to support the development of porous media operating under the conditions of hydrogen–ammonia combustion.

© 2026 The authors. This is an open access article under the Creative Commons Attribution 4.0 International License (https://creativecommons.org/licenses/by/4.0/).

Keywords: High-temperature porous ceramics; Thermal shock resistance; Hydrothermal corrosion; Environmental barrier coating; Triply periodic minimal surface (TPMS); Additive manufacturing

1. Introduction

Driven by global carbon neutrality goals, major economies have increasingly incorporated hydrogen-ammonia fuels into their national strategic plans. In 2020, the European Union unveiled its *European Hydrogen Strategy*, which set a clear objective to deploy at least 40 GW of renewable hydrogen electrolysis capacity by 2030 and identified ammonia as a key pathway for hydrogen carriers and zero-carbon fuels [1]. In its *Basic Hydrogen Strategy*, Japan's Ministry of Economy, Trade and Industry has been actively advancing commercial demonstration projects for ammonia-based power generation; Mitsubishi Heavy Industries (MHI) and IHI (Ishikawajima-Harima Heavy Industries) have each achieved demonstration operations with a 20% ammonia blending ratio in large gas turbines [2]. The Australian Renewable Energy Agency (ARENA) has funded multiple green ammonia production and export projects to establish an ammonia supply chain across the Asia-Pacific region [3]. According to the International Energy Agency (IEA) 2022 Global Hydrogen Review, porous media combustion technology is recognized as one of the core enabling technologies for clean hydrogen–ammonia combustion because of its heat storage and regeneration capabilities and low-emission characteristics [4].

Porous media combustion technology places reaction zones within inert porous skeletons and realizes internal heat recuperation through coupled solid conduction and thermal radiation. Despite its attractive application prospects for zero-carbon hydrogen and ammonia fuels, this technology imposes extremely harsh service loads on porous components [5–8]. The three-dimensionally interconnected porous high-temperature skeletons endure long-term exposure at 900–1500 °C, water-vapor-rich oxidizing atmospheres originating from ammonia combustion, and repeated thermal cycling induced by high-velocity hydrogen flow. Such aggressive environments readily cause material degradation modes including high-temperature sintering, thermal-shock cracking, hydrothermal corrosion, oxidation, and progressive loss of mechanical strength of solid struts [9–11].

1.1. Materials and Methods

Search Strategy: This study was conducted in accordance with the PRISMA (2020) guidelines [12]. The search databases included VIP, Web of Science, Elsevier, CNKI, *etc.*, and the search period was 1995 to 2026. Chinese search terms: porous medium combustion, porous ceramics, thermal shock resistance, high-temperature porous medium materials, hydrogen-ammonia combustion, additive manufacturing, porous medium structures, material failure and protection, porous ceramics preparation processes, silicate refractory materials, oxides, non-oxides, low carbon emissions, low nitrogen oxide emissions. English search terms: High-temperature porous ceramics, thermal shock resistance, hydrothermal corrosion, environmental barrier coating, EBC, triply periodic minimal surface, TPMS, additive manufacturing, porous media combustion, hydrogen and ammonia combustion, clean combustion of zero-carbon fuels, excess-enthalpy combustion, high-temperature porous media materials. Search query example using CNKI: SU = ('porous media combustion' + 'porous burner' + 'excess-enthalpy combustion') OR SU = ('hydrogen' + 'ammonia') AND SU = ('porous ceramics' + 'silicon carbide' + 'silicon nitride' + 'mullite' + 'cordierite' + 'refractory materials' + 'intermetallic compounds'). Supplementary search queries: SU = ('thermal shock' + 'thermal shock resistance' + 'steam corrosion' + 'hydrothermal corrosion') OR SU = ('silicon carbide' + 'porous ceramics') AND AB =('combustion'); SU = ('additive manufacturing' + '3D printing' + 'photopolymerization') AND SU = ('porous' + 'lattice' + 'ultra-smooth surfaces' + 'TPMS'). Specifically: Records were retrieved from the following databases: WoS (n = 554), Elsevier (n = 870), CNKI (n = 1558),

VIP (n = 1651), and other databases (n = 70); the total number of records across all databases was n = 4703; after removing duplicates, the number of remaining records was 2967; following title-and-abstract screening, the following records were excluded: 1259 articles unrelated to porous medium combustion; 305 articles concerning service materials not operated within the specified temperature range; and 403 non-research-related documents, such as patents or news articles. Full-text searches failed for 1000 articles; following full-text assessment, an additional 893 references were excluded. The exclusion criteria were as follows: studies not covering high-temperature operating conditions of 900–1500 °C (n = 153); studies not involving hydrogen/ammonia or near-zero-carbon fuel-related research (n = 177); studies reporting only combustion/emission characteristics without providing material performance data (n = 173); duplicate publications or studies with incomplete data (n = 108); and 282 articles for which full texts were inaccessible. The final number of studies included in this review was n = 107. For the detailed procedure, refer to Figure 1.

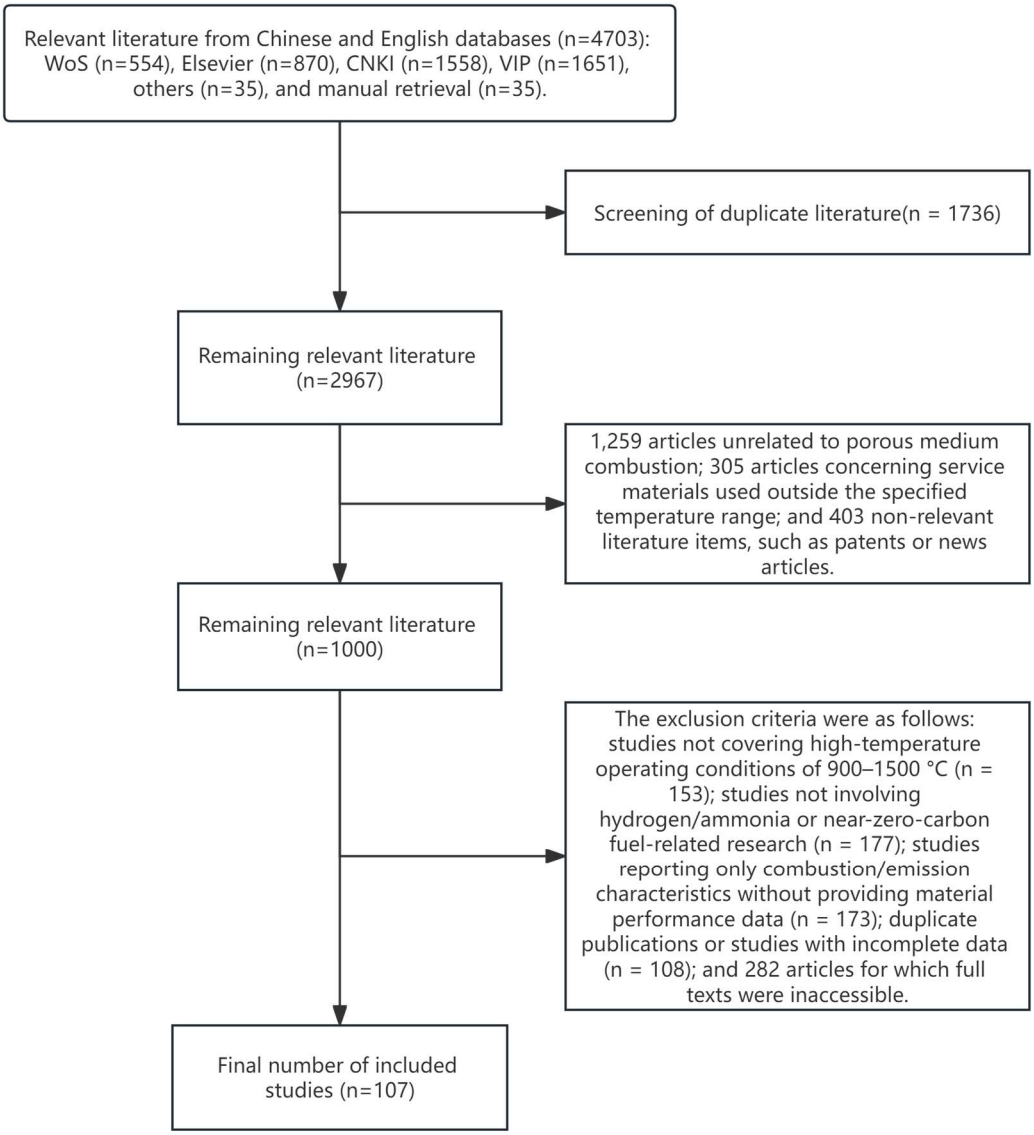


Figure 1. Literature screening flowchart.

Within the scope of the 107 studies retrieved under the search protocol of Section 1.1 and the three review streams summarized in Section 1, the coupled oxidation–volatilization failure of SiC skeletons in

water-vapor-rich atmospheres (Section 5), the defect-to-crack evolution introduced by different fabrication routes (Section 4), and a closed-loop fuel–material–topology–coating selection logic (Sectipon 6) have not, to the authors' knowledge, been synthesized in a single review. These claims are bounded by the search scope and cut-off date stated in Section 1.1.

Among these, the concurrent oxidation–volatilization failure of silicon carbide (SiC) frameworks under a humid steam atmosphere involves two key aspects: the water vapor corrosion mechanism and the oxidation kinetics of SiC, as well as protective coating systems. There are 12 references pertaining to the water vapor corrosion mechanism and SiC oxidation kinetics [9,11,13–22], and 10 references concerning protective coating systems ([23–32].

The mechanisms by which defects evolve into cracks under different fabrication processes encompass three categories: inherent defects of conventional fabrication processes, defects associated with additive manufacturing, and thermal shock-induced cracking and crack propagation. There are 7 references related to inherent defects of conventional fabrication processes [33–39]; 12 references related to additive manufacturing defects [40–51]; and 13 references related to thermal shock-induced cracking and crack propagation [10,52–63].

There are 50 relevant references pertaining to the closed-loop decision-making logic for the selection of fuel, materials, topological structure, and coatings, namely [2,5,7,8,23,64–108].

Over the past two decades, a substantial body of review literature has addressed porous media combustion technology from multiple perspectives. These prior contributions can be broadly categorized into three streams.

The first and most established stream centers on combustion reaction kinetics and flame stabilization. Reviews in this category have systematically elucidated the fundamental mechanisms governing flame propagation, stabilization limits, and extinction behavior within porous media. They have established theoretical frameworks for excess-enthalpy combustion, clarified the roles of solid-phase heat recirculation and radiation feedback in extending lean flammability limits, and provided parametric correlations linking equivalence ratio, pore density (PPI), and flow velocity to flame stability boundaries. Representative contributions include comprehensive treatments of premixed flame anchoring mechanisms in packed beds and ceramic foams, as well as numerical modeling frameworks for predicting combustion efficiency in porous burners [6,64].

The second stream focuses on pollutant emission control and combustion limit modulation. These reviews have quantified the relationship between porous media operating parameters (porosity, pore size, inlet velocity) and pollutant species concentrations (NO_x, CO, unburned hydrocarbons). They have demonstrated that porous media combustion can achieve ultra-low NO_x emissions under lean conditions and have proposed operational strategies—including equivalence ratio optimization, inlet preheating, and multi-section burner design—for minimizing emissions while maintaining flame stability [7,65,66].

The third, more recent stream addresses flow-field regulation and computational fluid dynamics (CFD) modeling of reactive flows within porous structures. These works have advanced the understanding of gas-solid heat transfer, local thermal non-equilibrium effects, and the coupling between fluid dynamics and chemical kinetics in complex porous geometries [5,8].

Despite these significant advances, a critical analysis indicates that existing reviews commonly treat the porous skeletal material primarily as an inert, thermally passive medium whose structural integrity is assumed to remain intact throughout service. In doing so, they address material-centric challenges that are decisive for practical deployment and long-term reliability of porous media combustion technology less explicitly:

(1) High-temperature material degradation mechanisms. The coupled processes of sintering-induced pore closure, progressive oxidation, hydrothermal corrosion (particularly severe under ammonia combustion atmospheres with ~20–30% water vapor), and thermomechanical fatigue cracking have not been systematically reviewed within the context of porous media combustion service. The

structure–property–failure relationships governing skeletal material performance under 900–1500 °C cyclic thermal loading remain fragmented across disciplinary boundaries [9–11].

(2) Topological thermomechanical failure analysis. While prior reviews have discussed how pore architecture influences flame behavior, they have not examined how topology governs thermal stress distribution, stress concentration, and crack propagation pathways within the skeletal framework. The thermomechanical coupling between intrinsic material parameters (thermal expansion coefficient, elastic modulus, Poisson's ratio) and topological design variables (cell geometry, strut thickness, tortuosity) has not been quantitatively addressed.

(3) Manufacturing-induced micro-defects. The stochastic and systematic micro-defects introduced by different fabrication routes—including hollow struts from replica foam impregnation, interlayer delamination from additive manufacturing, and insufficient densification from incomplete sintering—directly determine the initial structural integrity and subsequent degradation trajectory of porous components. No prior review has catalogued these process-induced defects and their implications for high-temperature service performance.

(4) Surface protection strategies. The necessity, design principles, and comparative effectiveness of protective coatings for porous skeletons operating in hydrogen–ammonia combustion atmospheres have not been comprehensively evaluated. In particular, the hydrothermal volatilization-corrosion mechanism specific to SiC in water-vapor-rich environments and the corresponding multilayer coating solutions (mullite, cordierite, Al_2O_3–Cr_2O_3 solid solution, rare-earth silicate systems) remain scattered across primary research articles without integrative synthesis.

(5) Fuel–material–topology–coating synergistic selection. No existing review has proposed a unified decision framework that maps fuel combustion characteristics to dominant material failure modes, then to targeted coating protection strategies, and finally to compatible topological architectures. This cascading logic—from fuel type to material selection to structural design to protective modification—represents a critical gap in translating lab-scale porous media combustion research to engineering practice.

The present review is explicitly designed to address these five gaps. Unlike prior reviews that adopt combustion behavior as the central organizing principle, this work takes the extreme material service conditions of hydrogen–ammonia combustion as boundary constraints and constructs a full-chain research logic spanning material intrinsic thermophysical properties → topological thermomechanical response → manufacturing-induced defects → service degradation mechanisms → coating protection strategies → synergistic fuel–material–topology–coating selection framework. This orientation represents a deliberate conceptual inversion: rather than asking "how does porous media affect combustion?", we ask "how does the combustion environment degrade the porous medium, and how can the material system be co-designed to survive it?". This perspective has not been systematically articulated in any prior review (Table 1).

Table 1. Structured comparative table of the review content.

Category	The Main Contributions of This Review	Existing Limitations or Gaps in the Review	Unique Value
Combustion Kinetics and Flame Stability [33]	A theoretical framework for the flame anchoring mechanism has been established, and parametric correlations between equivalence ratio, pore density, and flow velocity have been derived [6]	Treat the porous skeleton as an inert/passive medium, and analyze the degradation behavior of the unprocessed material under service conditions [64]	A bidirectional coupling relationship between material degradation and combustion performance is proposed and discussed (Section 6.4)
Pollutant emission control [7,67]	Quantified the emission-parameter relationship and proposed a multi-stage burner design to reduce emissions [65,66]	Coating modification was not incorporated into the material design; catalytic functionality was not integrated	The concept of "catalytic–flame-retardant integration" was proposed

Flow Field Control and CFD Simulation [52]	Computational models for gas-solid heat transfer and local thermal non-equilibrium have been developed [5,8]	The effects of manufacturing-induced defects on the actual flow path and thermal contact have not been considered [89]	The system catalogs manufacturing-induced microdefects and analyzes how these defects evolve into stress concentration sites and crack initiation sites under high-temperature cycling, thereby providing defect input data for more realistic computational models
Review of Refractory and Ceramic Materials [68]	A thermophysical property database for various material systems has been provided, along with recorded data on oxidation kinetics and thermal shock resistance [33,61]	Material properties were not systematically compared under the specific service requirements of hydrogen-ammonia combustion; furthermore, a material–topology–coating synergistic framework is lacking [22,63,106]	Under identical topological configuration and temperature differential ΔT, the thermal stress in SiC is approximately 60% of that in Al_2O_3 (Section 3.1; dense, high-purity test specimens [4,56,57]); consequently, the thermal shock resistance parameter R of SiC (≈273 K) is substantially higher than that of Al_2O_3 (≈115 K) (Section 3). A fuel–material–topology–coating cascade selection matrix is proposed
Review of Ceramic Additive Manufacturing [69]	Documented AM's capability to fabricate complex topologies; documented achievable geometric precision [44,46]	The study focuses on room-temperature mechanical properties and geometric precision; however, it does not address high-temperature defect evolution or thermal cycling durability [49,50]	This study specifically analyzes AM-specific micro-defects as potential sources of high-temperature crack initiation, and evaluates their impact on the thermal shock life under simulated porous medium combustion conditions.
This text	Establish a full-chain logical framework encompassing "structure–performance–failure–application"; quantify the coupling between material and topology based on R (Section 3.1); evaluate multilayer coating protection for SiC substrates (Sections 5.1–5.4); and propose a synergistic selection matrix (Section 6)	Composite material systems, self-healing coatings, large-scale additive manufacturing, multi-scale numerical modeling, and industrial standardization remain open challenges (Section 7.2)	(1) A topology–material co-design criterion based on the thermal shock resistance parameter R, substantiated by the parameter data of Section 3 and the stress analysis of Section 3.1; (2) the coupled oxidation–volatilization corrosion mechanism of SiC under NH_3/H_2O conditions, established in Section 5 on the basis of the oxidation kinetics of Section 5 and the coating results of Sections 5.1–5.4; (3) a fuel–material–topology–coating synergistic selection matrix (Section 6), integrated into the full-chain design framework of Section 6.

(1) The topology–material co-design criterion based on the thermal shock resistance parameter R is substantiated by the parameter data of Section 3 and the stress analysis of Section 3.1; (2) the coupled oxidation–volatilization mechanism of SiC under NH_3/H_2O conditions is established in Section 5 on the basis of the oxidation kinetics reported in Setion 5 and the coating results of Sections 5.1–5.4; (3) The fuel material–topology–coating co-selection matrix has been integrated into the full-chain framework of Section 6.

"Bidirectional coupling" denotes the two-way interaction in which the combustion environment drives material degradation (sintering, oxidation, hydrothermal corrosion, thermal-fatigue cracking), while the evolving skeletal structure in turn modifies flame stability, radiative output, and pollutant formation. "Catalytic–flame-retardant integration" denotes a porous skeleton that simultaneously anchors the flame through its thermal-regeneration function and hosts catalytic phases for in-situ fuel decomposition and NO_x

removal (Section 6.2). Both concepts are proposed as organizing hypotheses and require dedicated experimental validation.

As shown in Figure 2, unlike previous reviews that focus on combustion reactions and flow characteristics, this review uses the extreme material service conditions of hydrogen-ammonia combustion as boundary constraints. The work firstly aims to systematically sort out the structure-performance-failure relationships of existing high-temperature porous media, by correlating intrinsic material thermophysical properties, topological architectures, manufacturing-induced micro-defects and real-world degradation behavior under hydrogen-ammonia combustion environments. Secondly, it intends to summarize state-of-the-art hydrothermal corrosion mechanisms and available surface protection strategies for porous skeletons. On this basis, a synergistic material-topology-coating selection framework is expected to be established for practical material screening. It is anticipated that this review can offer material-oriented references to mitigate core bottlenecks restricting component service life, and facilitate the translation of lab-scale porous-media combustion technology toward practical low-carbon energy equipment.

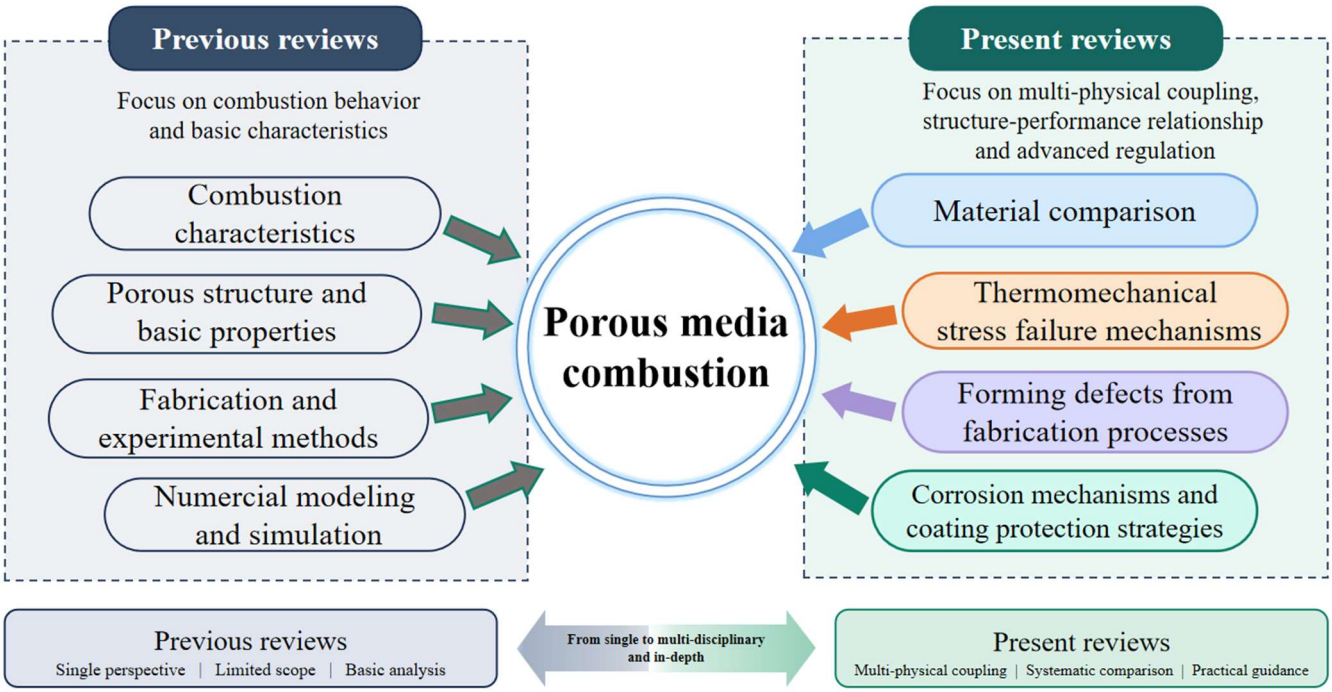


Figure 2. Schematic comparison between previous reviews (focusing on combustion behaviors) and the present review (focusing on high-temperature material degradation, topological failure, manufacturing defects, and coating protection under H_2/NH_3 combustion conditions).

2. Classification and Intrinsic Service Properties of High-Temperature Porous Media Materials

Selecting porous media materials is a multi-objective optimization task that balances high-temperature resistance, thermal shock resistance, thermal conductivity and radiative performance, chemical inertness, and economic cost. According to chemical composition, porous media materials can be classified into four principal categories: oxide ceramics, non-oxide ceramics, silicate refractories, and intermetallic compounds [23]. Table 2 provides a detailed listing of the performance characteristics of various materials.

Table 2. Comparison of key high-temperature service properties of four categories of porous media materials.

Material Type	High-Temperature Resistance	Thermal Shock Resistance	Thermal Conductivity/Radiative Performance	Chemical Stability/Oxidation Resistance	Mechanical Strength	Core Limitations
Oxide ceramics	Excellent	Poor	Poor	Excellent	Al_2O_3: high hardness but insufficient strength; ZTA: composites show excellent mechanical performance	Limited thermal shock service life
Non-oxide ceramics	Good	Good	Good	Poor	Si_3N_4/SiC: composites exhibit favorable mechanical properties;	SiC high-temperature oxidation
Silicate refractories	Moderate to low	Good	Moderate to good	Good	Mullite: when employed as an additive, can suppress coating cracking	Relatively low melting point
Intermetallic compounds	Good	Good	Moderate	Moderate long-term oxidation resistance	Ni–Al: stable under ultra-lean combustion CoCr diamond lattice: high structural rigidity	Cost and long-term oxidation resistance

2.1. Oxide Ceramics

Alumina (Al_2O_3) is the most extensively employed porous media material, featuring a melting point of approximately 2050 °C, favorable chemical stability, high hardness, and relatively low cost. Among the three commonly used material categories, Al_2O_3-based ceramic foam burners exhibit the highest temperature levels and superior flame stability [13]. Nevertheless, its intrinsic drawbacks, including moderate thermal conductivity (~30 W/(m·K)), low infrared emissivity (~0.3), and high thermal expansion coefficient (~8.0 × 10^{-6} K), lead to considerable thermal stress amplitude under cyclic thermal loads, resulting in unsatisfactory thermal-shock resistance and shortened service life under frequent start-stop conditions [14]. Improvement strategies include the introduction of micro-silica powder to promote the *in-situ* formation of elongated mullite crystals, thereby increasing the surface emissivity from 0.262 to 0.588 and elevating the burner surface temperature by approximately 225 °C, as well as the deposition of flower-like CeO_2 coatings, which raise the emissivity from 0.52 to 0.71 and extend the lean flammability limit to 3.5%. Despite the significant cost advantage of Al_2O_3, these intrinsic deficiencies limit its thermal shock resistance and service life under frequent start-stop or high power density operating conditions [15].

Zirconia (ZrO_2) possesses an ultra-high melting point (~2715 °C) and excellent chemical inertness, rendering it suitable for ultra-high-temperature applications. However, its extremely low thermal conductivity (~2–3 W/(m·K)) deteriorates thermal shock resistance. Stabilization with 3 mol% Y_2O_3 (3Y-ZrO_2) can enhance the mechanical properties, and it is frequently used in combination with zirconia-corundum composites [53]. Zirconia-toughened alumina (ZTA) composites combine the merits of both constituents and hold considerable promise for high-end applications. Nevertheless, the trade-off between melting point advantage and inferior thermal conductivity still restricts its standalone deployment as large-scale porous skeletons under cyclic thermal shock.

Chromia (Cr_2O_3) exhibits excellent high-temperature stability with a melting point of 2435 °C. It is rarely used as a standalone skeleton material and is mostly applied as Al_2O_3–Cr_2O_3 solid-solution protective coating on SiC substrates. The solid-solution coating with corundum-type crystal structure delivers a low oxygen diffusion rate. When deposited onto SiC skeletons and sintered at 1400–1500 °C, the coating

imparts an oxidation weight gain of merely 0.21–0.28% after 100 h of exposure at 1500 °C, with no delamination observed [16]. Nonetheless, the potential formation of volatile Cr_2O_3 at elevated temperatures and corresponding environmental toxicity concerns should not be ignored.

2.2. Non-Oxide Ceramics

Silicon carbide (SiC) offers a favorable combination of thermophysical properties among porous media materials. Its high thermal conductivity (~120 W/(m·K)) and low coefficient of thermal expansion (4.5×10^{-6} K) give SiC excellent thermal shock resistance and a relatively high infrared emissivity that exceeds that of oxide ceramics [17]. Excess-enthalpy combustion equipment based on SiC porous ceramics can achieve energy consumption reductions of nearly 50% and NO_x emissions below 30 mg/Nm^3. However, SiC is susceptible to oxidation in high-temperature oxygen- and water-vapor-enriched environments, forming SiO_2 scales that lead to strut thinning, strength degradation, and substantially reduced service life. The oxidation reaction intensifies markedly with increasing temperature between 1000 and 1500 °C, and in the presence of water-vapor, the formation of volatile $Si(OH)_4$ species accelerates corrosion [34]. Accordingly, SiC porous media typically necessitate the application of surface protective coatings. Consequently, surface protective coatings are indispensable for SiC-based porous skeletons working under hydrogen-ammonia combustion atmosphere [18].

Silicon nitride (Si_3N_4) is characterized by low density, high specific strength, high specific surface area, and excellent thermal stability. The performance of monolithic Si_3N_4 porous media is inferior to that of SiC; but, Si_3N_4/SiC composite porous ceramics achieve a compressive strength of 62.4 Mpa and a fracture toughness of 4.8 Mpa·m^(1/2) at 1200 °C with a porosity of 69.3%, while retaining approximately 91% of their strength after 100 thermal cycles [35]. This class of composites demonstrates substantial potential for structural-functional integration.

Molybdenum disilicide ($MoSi_2$) combines metallic and ceramic characteristics, with a melting point of 2030 °C and excellent high-temperature oxidation resistance afforded by the formation of a dense protective SiO_2 film. It is primarily employed in electrical heating elements and heat exchangers. Its porous forms (e.g., $MoSi_2$/SiC composites) can stably maintain porosities exceeding 50%, rendering them suitable for ultra-high-temperature burner applications [70]. Therefore, composite design is indispensable to mitigate thermal-stress risk for practical porous-media service.

Besides, the Ortona research group at the Politecnico di Torino, Italy, systematically investigated the early oxidation behavior of reaction-sintered SiC (RB-SiC) porous structures under an oxygen-enriched atmosphere at 1400 °C, revealing that preferential oxidation of residual silicon in the Si/SiC system leads to the formation of a self-healing SiO_2 protective layer on the skeleton surface; however, after prolonged service, volatilization of this SiO_2 layer results in gradual thinning of the skeleton [71]. The Studart research group at the Swiss Federal Laboratory for Materials Science and Technology (Empa), Switzerland, employed the ice-templating/freeze-casting method to fabricate SiC–ZrB_2 ultra-high-temperature porous ceramics featuring layered, directionally aligned pore structures, demonstrating approximately 40% improved oxidation resistance at temperatures above 1600 °C compared to conventional foam ceramics [72]. The Roos research group at the Karlsruhe Institute of Technology (KIT), Germany, fabricated high-density SiC porous components via silicon infiltration sintering and systematically evaluated their long-term thermomechanical stability in a steam-containing atmosphere [36].

2.3. Silicate Refractories

Mullite ($3Al_2O_3 \cdot 2SiO_2$) is characterized by uniform thermal expansion, excellent thermal shock resistance, and chemical corrosion resistance. In comparative studies of additively manufactured burners, $3Al_2O_3 \cdot 2SiO_2$ structures have demonstrated superior durability to Al_2O_3 [15]. When used as a secondary

additive phase, reactions between constituent phases in coal gangue generate mullite, which induces residual compressive stress within the coating to suppress crack propagation, thereby elevating the porous burner surface temperature by approximately 48 °C [73].

Although silicate refractories exhibit excellent thermal shock resistance, their relatively low melting points ($3Al_2O_3 \cdot 2SiO_2$ ~1850 °C, $2MgO \cdot 2Al_2O_3 \cdot 5SiO_2$ ~1460 °C) restrict their direct application as load-bearing skeletal materials in ultra-high-temperature zones (>1600 °C). Consequently, they are more commonly employed in synergistic combination with SiC and other materials in the form of coatings or composite phases [74].

Cordierite ($2MgO \cdot 2Al_2O_3 \cdot 5SiO_2$) is well-known for ultra-low thermal expansion coefficient (~1.5×10^{-6} K). Its most valuable merit for porous-media application is high infrared emissivity (0.85–0.9). Through vacuum infiltration, $2MgO \cdot 2Al_2O_3 \cdot 5SiO_2$ coatings can be deposited onto SiC skeletal surfaces, improving radiative heat transfer capacity. After thermal treatment at 1350 °C, the composite coating still maintains compressive strength of 1.18 Mpa with residual strength retention of 67%. Moreover, the burner surface temperature is elevated by approximately 140 °C, with concomitant significant reductions in NO_x and CO emissions [75].

Aluminum titanate (Al_2TiO_5) possesses an extremely low thermal expansion coefficient, yet monolithic sintered bodies suffer from low strength and brittle fracture. Composite fabrication with mullite (mass ratio 6–7:3–4), together with stabilizers such as MgO, SiO_2, or CeO_2 can balance thermal shock resistance and sintered mechanical performance [76]. Zircon ($ZrSiO_4$) decomposes at 1400 °C to generate ZrO_2 and SiO_2. Newly formed SiO_2 reacts with Al_2O_3 to generate mullite, and the phase transformation of ZrO_2 introduces a microcrack toughening effect to enhance thermal-shock performance [16].

2.4. Intermetallic Porous Materials

The Siberian Branch of the Russian Academy of Sciences developed Ni–Al-based intermetallic porous burners employing self-propagating high-temperature synthesis (SHS) technology. The two-stage configuration comprising fine pores (d = 0.65 mm) and coarse pores (d = 3.25 mm) achieved a turndown ratio exceeding 13.8 under the ultra-lean combustion condition of an equivalence ratio of 0.25, with efficiency markedly superior to that of conventional ceramic burners [77]. The Clyne group at the University of Cambridge, UK, utilized spark plasma sintering (SPS) to prepare Ti–Al intermetallic compound porous structures, demonstrating excellent high-temperature specific strength and creep resistance [78]. The research team at the Institute of Structural Macrokinetics and Materials Science (ISMAN), Russian Academy of Sciences, employed thermal-explosion mode of self-propagating high-temperature synthesis (SHS) to fabricate NiAl–Cr_2O_3 composite materials from Ni + Al + Cr_2O_3 reaction mixtures; by adjusting the Cr_2O_3 content in the reactant system, they systematically regulated the strength characteristics of the synthesized products and succeeded in obtaining a homogeneous NiAl-based material containing dissolved chromium and chromium oxide nanoparticles, with the micro-hardness, toughness, and residual porosity of the synthesized samples being characterized in detail [37]. Internationally, diamond lattice configurations fabricated from cobalt-chromium (CoCr) alloys have demonstrated enhanced flame stability and structural rigidity in upstream applications. Intermetallic compounds, which combine the toughness of metals with the high-temperature resistance of ceramics, represent a direction warranting further attention. However, systematic evaluation of manufacturing cost and long-term high-temperature oxidation resistance is still required before large-scale deployment.

Based on the above research, material intrinsic thermophysical parameters, including thermal expansion coefficient (α), thermal conductivity (λ), elastic modulus I, and oxidation resistance, determine thermal-shock behaviors. Nevertheless, practical high-temperature mechanical response of porous media is not only governed by chemical composition, but is also strongly modulated by topological architecture via thermal-stress redistribution and stress-concentration effect. The following section discusses thermos-

mechanical coupling failure covering traditional disordered structures and novel ordered porous configurations [54].

3. Thermo-Mechanical Coupling Failure of Porous Topological Structures Under Cyclic High-Temperature Conditions

The topological configurations of porous media govern the thermal stress distribution, thermal shock resistance lifetime, and gas-solid heat transfer efficiency. The evolutionary route of porous structures follows: disordered packed beds → ceramic foams → gradient structures → honeycomb/fiber architectures → lattice/TPMS configurations → topologically graded designs. Generally, a high structural ordering degree improves high-temperature service reliability [55].

In the field of applying ordered porous structures from additive manufacturing to combustion applications, the research team led by Professor Abu Al-Rub at Khalifa University in the United Arab Emirates has conducted systematic studies on the thermos-fluidic-solid coupled behavior of TPMS porous structures. Al-Ketan et al. fabricated metal porous burners based on Gyroid and Primitive TPMS architectures; experimental results demonstrated that the Gyroid structure achieved a combustion stability range approximately 35% wider than that of random foams in methane-air premixed combustion, while the uniformity of wall temperature distribution was improved by approximately 50% [56]. The research group led by Jeng at Singapore University of Technology and Design (SUTD) fabricated Diamond-and I-WP-type TPMS stainless steel porous heat exchangers using Selective Laser Melting (SLM), and systematically investigated the effects of specific surface area and tortuosity on the Nusselt number and pressure drop [57].

It should be emphasized that practical engineering application of TPMS and topologically-graded structures heavily depends on manufacturing innovation. Conventional processes (e.g., the replica foam impregnation method) are incapable of realizing such complex geometries, whereas additive manufacturing techniques (e.g., lithography-based ceramic manufacturing, LCM), despite their capacity for precision forming, face challenges related to cost, achievable build dimensions, and sintering densification [79]. The structure-property relationships described in this section are predicated upon currently attainable fabrication processes, and are intended to provide topological design guidance for subsequent process optimization. Figure 3 provides a detailed overview of the developmental history of porous media structures, along with the respective advantages and disadvantages of each configuration.

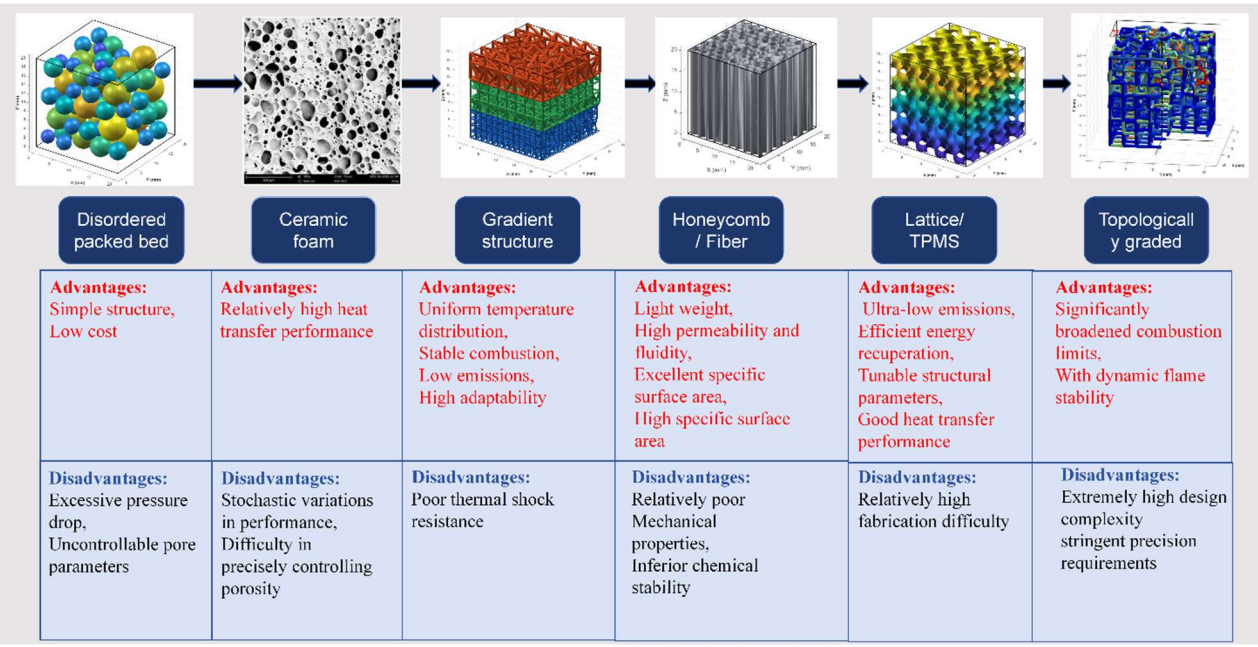


Figure 3. Evolution of porous topological architectures and their thermomechanical characteristics at high temperature.

3.1. Regulatory Effect of Intrinsic Material Properties on Thermomechanical Stress Response

The classical thermal-stress amplitude formula is expressed as:

$$\sigma_{th} = \frac{E \times \alpha \times \triangle T}{1 - \nu} \quad (1)$$

where σ_{th} represents the thermal stress, measured in Pa. E is the Young's modulus, which characterizes the stiffness of the material. α is the coefficient of thermal expansion, which characterizes the degree of expansion/contraction of the material with temperature change. ΔT is the change in temperature. ν denotes Poisson's ratio, which characterizes the ratio of transverse contraction or expansion of a material under tension or compression.

Taking SiC and Al_2O_3 as representative examples: under identical topological configurations and temperature differential ΔT, the thermal stress in SiC (E ≈ 400 GPa, α ≈ 4.5 × 10^{-6}/K, ν ≈ 0.16) is approximately 60% of that in Al_2O_3 (E ≈ 380 GPa, α ≈ 8.0 × 10^{-6}/K, ν ≈ 0.22) [80]. Therefore, diamond-lattice or Diamond-TPMS configurations deliver better crack-suppression performance when fabricated with SiC rather than Al_2O_3.

The thermal shock resistance factor represents the maximum temperature difference that a material can withstand without being damaged by thermal shock, in Equation (1), ΔT equals the value of R, and the values of σ_{th} and σ_f in Equation (1) are equal. The thermal shock resistance parameter $R = \sigma_f(1 - \nu)/(\alpha E)$ quantitatively reflects material intrinsic capability against thermal-shock fracture [81]: SiC shows much higher R (~273 K) compared with Al_2O_3 (~115 K) [82]. The above data represent the performance characteristics of high-density, high-purity ceramic test materials fabricated from SiC, Al_2O_3, and ZrO_2, as measured under room-temperature conditions and during thermal expansion tests conducted over a temperature range from 25 °C to 1000 °C. Accordingly, topologies with inherently high thermal shock resistance (e.g., Diamond-type TPMS, Kelvin cell structures) should be preferentially coupled with materials exhibiting low α and moderate E (such as SiC and mullite) to achieve optimal thermo-mechanical synergy. This synergy criterion establishes a material-intrinsic constraint perspective for the subsequent high-temperature mechanical comparison of different topological configurations [19]. Even for identical topological geometry, thermal-shock discrepancies among different materials originate from material *R* values amplified by geometric stress-concentration effects. Table 3 provides a detailed listing of the thermodynamic properties of various materials.

Table 3. Comparative summary of thermal shock resistance parameter (R) and thermal conductivity (λ) values.

Material	Representative Flexural Strength σ_f (MPa)	Elastic Modulus E (GPa)	Poisson's Ratio ν	Coefficient of Thermal Expansion α (×10^{-6} K)	Thermal Shock Resistance Parameter R (K)	Thermal Conductivity λ (W/(m·K))	Overall Thermal Shock Resistance Characteristics
$Al_2O_3 \cdot TiO_2$	100	130	0.25	0.5	~1154 (Extremely high)	0.86–1.5	Highest theoretical R value, but relatively low strength [83]
$2MgO \cdot 2Al_2O_3 \cdot 5SiO_2$	200	120	0.25	1.5	~833 (Very high)	1.2–1.8	Excellent thermal shock resistance [58]
Si_3N_4	950	310	0.26	3.2	~708 (High)	14–34	Well-balanced combination of strength and thermal conductivity, yielding outstanding thermal shock resistance [59]

3Y-TZP	1200	210	0.3	10.5	~381 (Moderate)	~2.0 (8YSZ: 1.9)	Actual crack resistance exceeds the calculated prediction [84]
SiC	600	410	0.16	4.5	~273 (Moderately high)	120–200 (Exceptionally high)	High thermal conductivity facilitates rapid thermal stress dissipation
$3Al_2O_3 \cdot 2SiO_2$	250	200	0.25	4.5	~208 (Moderate)	0.55–1.52	Relies on microcrack toughening for compensation [85]
Al_2O_3	450	380	0.22	8	~115 (Relatively low)	25–45	Actual water-quench test ΔT of approximately 200–250 K
$MoSi_2$	450	440	0.17	8.5	~100 (Very low)	~46.5 (composite)	Heating elements rely on compositing for performance enhancement

3.2. Thermal-Shock Failure Mechanism of Conventional Disordered Porous Structures

Granular packed beds and ceramic foams fabricated via the replica foam impregnation method are susceptible to localized stress concentration under cyclic thermal shock owing to the stochastic nature of strut dimensions, morphologies, and spatial distributions. During the replication of polyurethane sacrificial templates, residual hollow defects frequently persist within the foam struts, thereby diminishing the thermal shock resistance parameter. The introduction of gradient structures-such as an axial configuration comprising a small-pore preheating layer combined with a large-pore combustion layer, can markedly improve thermal stress distribution. For example, a three-layer gradient design elevates the main combustion zone temperature by 61–117 K and increases the excess-enthalpy temperature by 80–100 K relative to dual-layer configurations, while simultaneously suppressing flame migration and reducing interlayer cracking induced by thermal gradients. The Trimis team at the German Aerospace Center (DLR) pioneered fundamental theoretical and applied research on porous medium combustion. This team proposed the conceptual framework of "excess enthalpy combustion" and, by employing a dual-layer gradient pore size design, achieved near-zero emissions in hydrogen-air premixed combustion [86]. Furthermore, Gao et al. systematically compared the combustion characteristics of methane/air premixed mixtures in a two-layer porous burner packed with four different cellular foam materials—Al_2O_3, ZrO_2, iron-chromium-aluminum (FeCrAl), and silicon carbide (SiC)—in terms of flame stability, flame temperature, and pollutant emissions, providing a basis for the selection of foam materials for porous media burners [40]. Studies have demonstrated that a porosity reduction of approximately 8% can double the compressive strength; furthermore, through optimization of the strut diameter (from 1.4 to 2.0 mm), the compressive strength can be enhanced to 0.60 MPa while reducing the surface temperature by only 12.7 °C, thereby achieving a favorable synergy between mechanical and thermal performance [87]. Figure 4 shows the temperature variation curves for the single-layer, double-layer, and three-layer configurations in the premixed zone, combustion zone, and radiation zone.

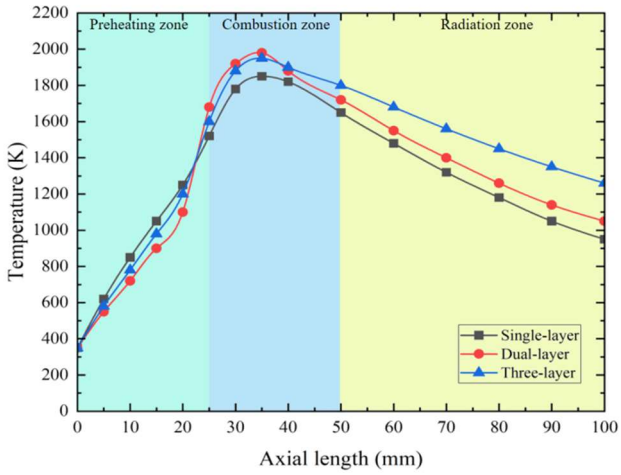


Figure 4. Axial temperature distribution of different gradient structures, showing thermal boundary conditions for thermomechanical analysis.

3.3. Thermo-Mechanical Coupling Behavior of Ordered Lattice and TPMS Structures

Additive manufacturing has enabled the realization of precisely controllable structures such as Kelvin cells, diamond lattice configurations, rhombic dodecahedra, and triply periodic minimal surfaces (TPMS). These structures eliminate stochastic variability, yielding more uniform thermal stress distributions, and permit quantitative regulation of thermomechanical performance through structural parameter design.

TPMS structures (Diamond, Gyroid, I-WP, Primitive) (Figure 5) feature high specific surface area and sharp-corner-free geometry. Structures with Kelvin cells can reduce CO and NO_x emissions by 60–70% compared with random foams, with a broader flame-stability temperature range [88]. Diamond lattice configurations can enlarge the energy recuperation efficiency to 82% under lean-burn conditions, with post-thermal-cycling structural rigidity superior to that of ceramic foams [60]. Rhombic dodecahedra achieve a broad stability range spanning equivalence ratios of 0.6–1.6 in ammonia-methane co-combustion, with a peak NO reduction of 450 ppm [89]. TPMS structures (Diamond, Gyroid, I-WP, *etc.*) feature high specific surface areas, and the absence of sharp edges, Diamond and I-WP types demonstrate superior flame stability compared with Gyroid and Primitive types. A hybrid Gyroid + I-WP topology can elevate the blow-off limit by 30% and the flashback limit by 40%. Alumina Gyroid-type TPMS structures fabricated via fused granulate printing remain intact after five thermal cycles of 1100 °C heating followed by air quenching [41]. Topologically graded structures-featuring spatially continuous transitions between lattice types-can increase the flame extinction limit by over 50%, with a substantially enhanced power dynamic range [38]. Thermal stress simulations have demonstrated that TPMS structures possessing higher tortuosity and specific surface area (particularly the Diamond type) exhibit lower thermal strain at equivalent porosity, attributable to a more uniform load distribution across the skeletal framework [39].

Thermal shock resistance of additively manufactured ceramic architectures has been evaluated by water quenching and in-situ characterization. For stereolithography (SLA)-fabricated Al_2O_3 and ZrO_2 lattice structures, thermal shock tests revealed that the lattice architectures exhibited better thermal shock resistance than conventional foam counterparts. For Al_2O_3 ceramics fabricated by photopolymerization-based additive manufacturing, in-situ digital radiography during thermal shock has been employed to track damage evolution and evaluate thermal shock resistance [42].

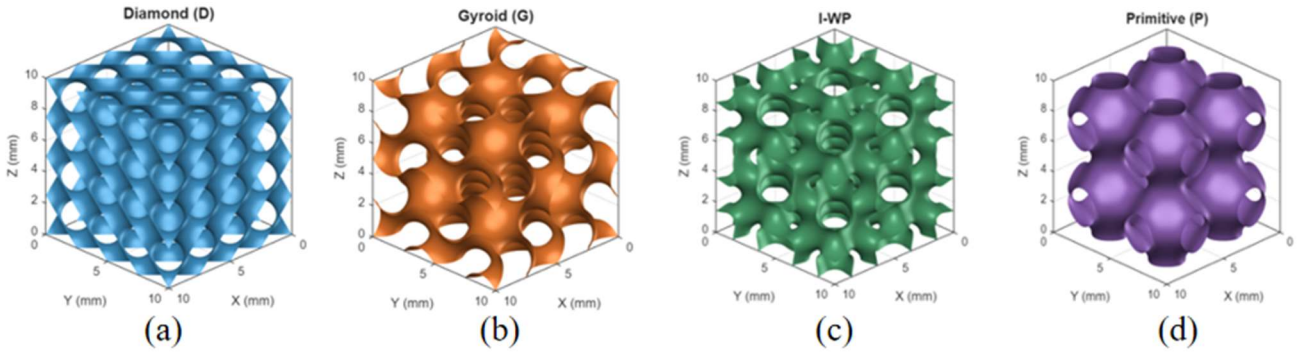


Figure 5. Three-dimensional renderings of representative TPMS topologies: (**a**) D; (**b**) G; (**c**) I-WP (W); (**d**) P.

Although ordered TPMS and topologically-graded structures exhibit promising thermomechanical properties, large-scale manufacturing still faces challenges including high cost and sintering distortion, which remain to be further solved. Structural design must consider manufacturing feasibility.

4. Fabrication-Induced Micro-Defects and Their Influence on High-Temperature Service Performance

Advanced topologies such as TPMS and gradient lattices possess favorable thermal-shock potential, yet their practical realization is fully restricted by manufacturing precision. Fabrication approaches not only determine whether target geometry can be realized, but also introduce characteristic micro-defects: hollow struts, interlayer delamination, insufficient densification[43]. These defects act as stress-concentration sites and crack initiation sources during high-temperature cyclic service. Manufacturing routes therefore directly determine microstructural integrity, mechanical strength, and high-temperature durability [44].

4.1. Inherent Limitations of Conventional Processes

The replica foam impregnation method is the most mature technique, capable of producing high-porosity (70–90%) components. However, the struts frequently exhibit a hollow internal architecture, which diminishes both mechanical strength and thermal shock resistance. Moreover, porosity and pore size are difficult to precisely control, resulting in poor batch-to-batch consistency [79]. Extrusion molding is employed for honeycomb ceramics and yields well-defined channel geometries; nevertheless, it is incapable of fabricating three-dimensionally interconnected open-cell structures [45]. The particle packing/sintering method enables pore size regulation through the incorporation of pore-forming agents; however, achievable porosity is inherently limited, and the process is susceptible to the introduction of impurities [46]. These conventional processes are incapable of fabricating complex gradient or TPMS configurations, and during the high-temperature sintering stage, grain coarsening, residual stress development, and strut defects are virtually unavoidable. Table 4 compares the advantages and disadvantages of the various preparation methods.

Table 4. Comparison of fabrication routes and their induced micro-defects for high-temperature porous media.

Fabrication Method	Porosity	Principal Advantages	Principal Limitations	Achievable Structures
Replica foam impregnation process	70–90%	The most mature and straightforward process, capable of producing high-porosity components	Reduced strength and thermal shock resistance, with porosity and pore size difficult to precisely control	Open-cell ceramic foams, three-dimensionally interconnected reticulated skeletons

Extrusion molding	20–60%	High dimensional accuracy, well-defined channel geometries, and exceptionally low flow resistance	Incapable of fabricating three-dimensionally interconnected open-cell structures	Honeycomb ceramics
Particle packing/sintering	30–60%	Relatively simple process with controllable pore size	Achievable porosity is inherently limited, and incapable of fabricating complex structures	Microporous ceramics
Direct foaming	Up to 90%+	Capable of producing ceramic foams with very high porosity	Difficulty in controlling the pore structure (open-cell vs. closed-cell)	High-porosity ceramic foams
LCM	45–95%	Fully controllable structural parameters; capable of realizing complex structures	Interlayer interfaces may serve as high-temperature crack initiation sites	TPMS, lattice, and arbitrarily complex structures
CVD	Dependent on the substrate material	Capable of producing high-purity, high-performance coatings or thin films	Complex equipment requirements, high cost, and relatively low production efficiency	Coating or thin-film-type porous structures

4.2. Advantages and Defect Challenges of Additive Manufacturing Technology

Technologies such as lithography-based ceramic manufacturing (LCM) and fused deposition/granulate printing have enabled the precise fabrication of complex topological configurations [47]. Mullite TPMS structures fabricated via LCM have demonstrated superior performance to alumina counterparts in thermal shock experiments, attributable to the lower coefficient of thermal expansion and higher fracture toughness of mullite [48].

Ceramic additive manufacturing exhibits prominent technical advantages in the fabrication of high-performance porous media. This advanced manufacturing technology enables precise regulation of structural parameters, which provides reliable technical support for exploring the intrinsic structure-property relationship of porous materials [49]. It also enables fabrication of continuous-gradient and topologically graded geometric configurations, allowing targeted optimization of internal thermal stress distribution within porous skeletons and effectively shortening the overall research and development cycle for novel porous media materials and structures (Figure 6).

In recent years, the industrialization of ceramic additive manufacturing technologies has accelerated significantly. The lithography-based ceramic manufacturing (LCM) technology developed by Austrian company Lithoz has enabled high-precision shaping of materials such as alumina, zirconia, and mullite, achieving layer thickness precision of up to 25 μm and density exceeding 99% of the theoretical density [50]. Recent industrial ceramic 3D printers provide the hardware basis for large-scale production of engineering-grade ceramic components.the Austrian company Lithoz launched the CeraMax Vario V900, based on Layerwise Intermediate Slurry (LIS) technology, which is the first 3D printer able to process dark ceramics such as silicon carbide with full density (build platform 250 × 250 × 290 mm) [51]. Eckel et al. from HRL Laboratories in the United States reported in *Science* the use of stereolithography with preceramic polymer precursors to obtain dense SiOC and SiCN ceramic structures after high-temperature pyrolysis; this approach effectively avoids the issues of debinding and cracking commonly encountered in conventional slurry-based curing processes [20].

Nevertheless, current ceramic additive manufacturing techniques still face several practical challenges in high-temperature service applications. The printed ceramic components commonly suffer from inadequate densification, and the inherent interlayer interfaces formed during printing tend to become crack initiation sources under long-term high-temperature thermal cycling, severely compromising structural integrity and service stability. In addition, the low production efficiency and high manufacturing cost restrict the large-scale preparation of large-size porous components, and the complex debinding and sintering post-processing procedures bring inevitable risks of component deformation and cracking. To

address these bottlenecks, subsequent research is supposed to develop special ceramic feedstocks adapted to additive manufacturing and establish mature integrated printing-sintering technical workflows, so as to improve the forming quality and high-temperature service performance of additively manufactured porous media [24].

Zhang et al. systematically investigated the printing process of Al_2O_3 ceramics fabricated via vat photopolymerization (VPP) additive manufacturing, using X-ray computed tomography (X-CT) to quantitatively characterize the three-dimensional morphology, distribution, and formation mechanisms of internal defects in both green and sintered bodies. Pore defects were identified in the green bodies, whereas both pore and delamination defects appeared in the sintered bodies. An orthogonal experimental design revealed that slicing thickness had the most significant effect on the flexural strength of the sintered Al_2O_3, followed by irradiance, with exposure time having the least influence; an appropriate slicing thickness (100 μm) enhances interlayer bonding through sufficient secondary photopolymerization, thereby suppressing delamination defects. By coupling defect control with process optimization (12,000 μW/cm², 4 s, 100 μm), a pathway from defect control to mechanical enhancement was established, and X-CT was validated as an effective non-destructive evaluation tool for ceramic additive manufacturing [25]. Previous studies have shown that the densification process and pore distribution of SiC-based ceramics are highly sensitive to the sintering schedule and heating mode: lower heating rates and higher sintering temperatures favour densification, whereas the rapid heating associated with microwave sintering may introduce micro-cracks and alter the mechanical response [26].

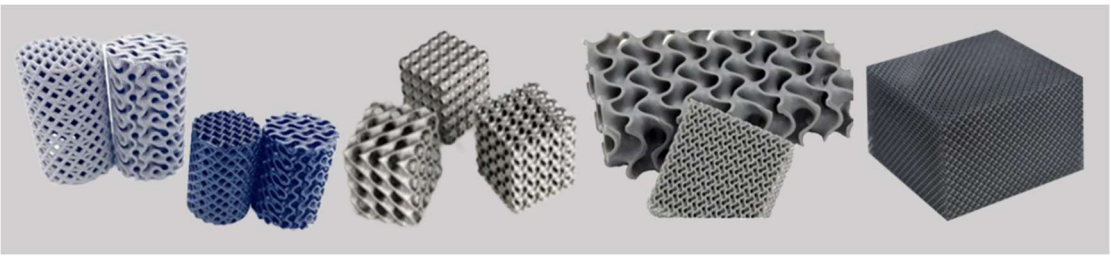


Figure 6. Photographs of additively manufactured TPMS structures.

The fabrication process governs the initial quality of the porous medium-including strut densification, defect distribution, and dimensional accuracy-whereas the service life is ultimately dictated by chemical degradation and thermo-mechanical coupling damage processes under high-temperature operating environments [27]. Having established the intrinsic material properties, topological configurations, and fabrication constraints, the following discussion will focus on oxidation kinetics, hydrothermal corrosion, and thermal shock failure mechanisms under actual combustion conditions, particularly those characterized by high water-vapor content and alternating thermal flux.

5. Hydrothermal-Oxidation Corrosion Mechanism and Protective Coating Strategies for Porous Media Materials

High water-vapor partial pressure originating from hydrogen-ammonia combustion induces severe material degradation, especially for SiC-based porous skeletons. SiC oxidation in dry air follows parabolic kinetics. In water-vapor-rich atmosphere, two dominant reactions proceed:

$$SiC(s) + 3H_2O(g) = SiO_2(s) + CO(g) + 3H_2(g) \quad (2)$$

$$SiO_2(s) + 2H_2O(g) = Si(OH)_4(g) \quad (3)$$

Reaction (2) causes volatilization of the protective SiO_2 scale layer and accelerates overall material degradation. Dense surface coatings with low oxygen- and water-vapor diffusivity become critical solution

for extending service lifetime of SiC porous components. Most reported coating performances are obtained from laboratory-scale specimens; achieving uniform coating covering complex inner surfaces of high-porosity porous skeletons remains a practical challenge (Figure 7) [90].

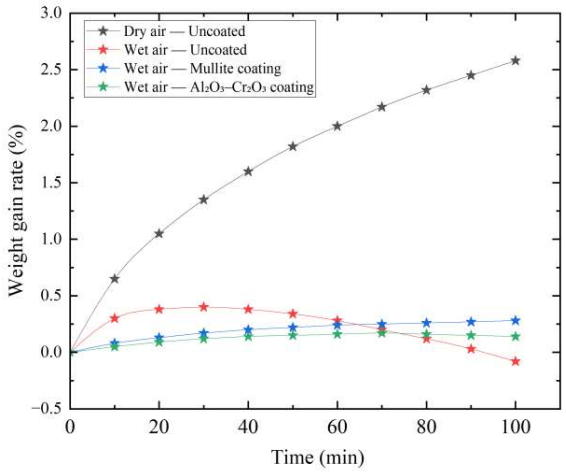


Figure 7. High-temperature oxidation weight gain curves of SiC porous ceramics.

5.1. Mullite-Based Protective Coatings

The coefficient of thermal expansion of mullite (5.3×10^{-6} K) is well matched with that of SiC (4.5×10^{-6} K), and mullite exhibits a low oxygen diffusion coefficient [28]. Through vacuum infiltration combined with dip-coating processes, mullite coatings are constructed on SiC skeletal surfaces, elevating the residual strength retention from merely 27% for uncoated SiC to a remarkable 93.5%, while transforming the primary pore diameter from the micrometer scale to the submicrometer scale [29]. Mullite-ytterbium silicate (Yb_2SiO_5) bilayer coatings further enhance the resistance to water-vapor corrosion, owing to the even lower water-vapor permeability of Yb_2SiO_5 [30].

5.2. Cordierite Composite Radiation Coatings

Cordierite coatings serve not only a protective function but also substantially enhance radiative heat transfer through their high emissivity (~0.9). Upon constructing a three-layer architecture on SiC called cordierite coating-SiC skeleton-cordierite infiltration, the burner surface temperature is elevated by approximately 140 °C, accompanied by reductions in NO_x and CO emissions [16]. After thermal treatment at 1350 °C, the coating achieves a compressive strength of 1.18 MPa.

5.3. Al_2O_3–Cr_2O_3 Solid-Solution Anti-Corrosion Coatings

Leveraging the formation of a continuous solid solution between Al_2O_3 and Cr_2O_3, these coatings are dense and exhibit an exceptionally low oxygen diffusion coefficient. When deposited onto SiC skeletons, the oxidation weight gain is merely 0.21–0.28% after 100 h of exposure at 1500 °C, with no appreciable delamination observed (Figure 8) [66]. Nevertheless, environmental risk originating from volatile CrO_3 at high temperature should be carefully considered in practical application [31].

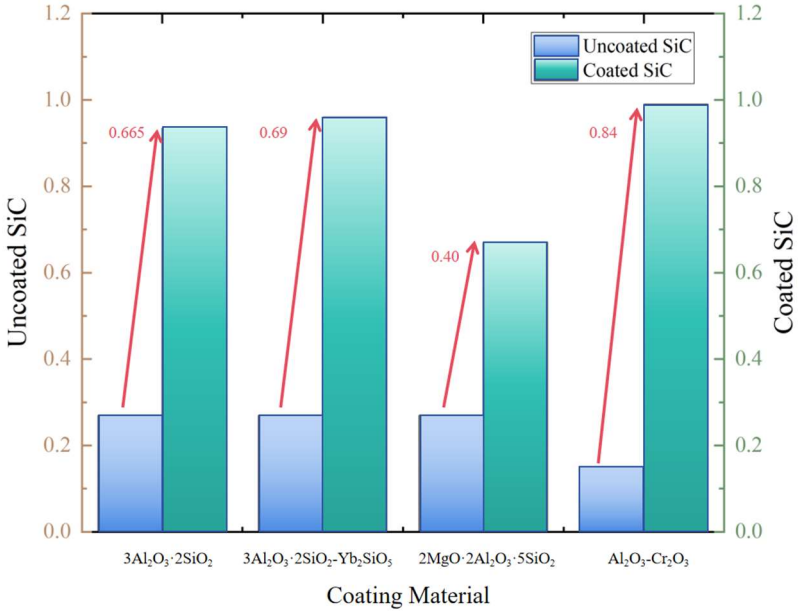


Figure 8. Comparative bar chart of residual strength before and after coating application.

5.4. Other Functional Coating Systems

Flower-like CeO_2 coatings deposited onto Al_2O_3 porous ceramics simultaneously provide high emissivity and catalytic activity, elevating the surface temperature to 1032.6 °C, increasing the heating rate by 29%, and reducing CO emissions to as low as 4.58 mg/m^3 [39]. Direct in situ reactive sintering of SiC skeletons to form mullite or cordierite also represents a viable pathway, offering the advantage of process simplification (Figure 9) [32].

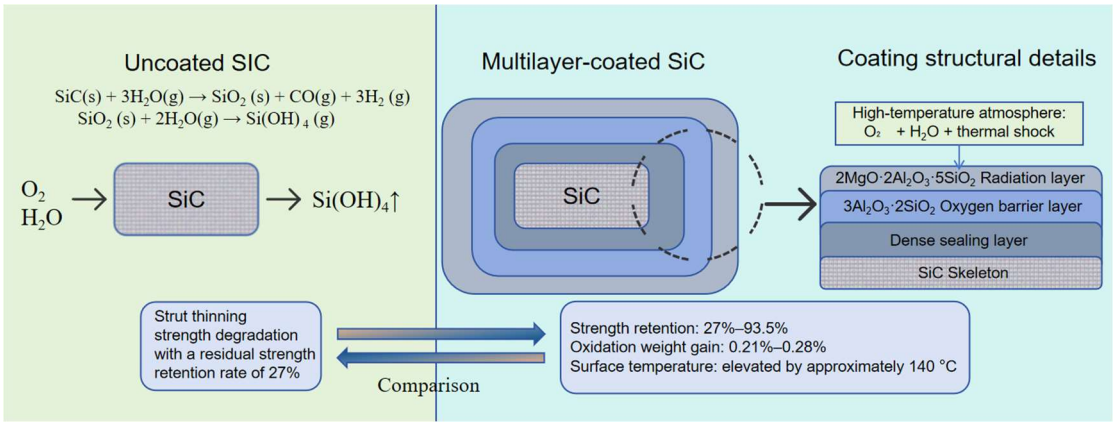


Figure 9. Cross-sectional schematic illustration of the coating protection mechanism.

International Frontier Research in Environmental Barrier Coatings (EBC): Extensive research experience has been accumulated in the application of Environmental Barrier Coating (EBC) technology for aero-engine C/SiC and SiC/SiC composite materials, and these findings provide valuable insights for the design of porous media coatings. To overcome the temperature limitation imposed by the melting point of the Si bond coating (~1414 °C), a bond-coat-free environmental barrier coating (EBC) was deposited on enhanced-roughness SiC substrates to assess coating adhesion for turbine applications beyond 1350 °C. Two EBCs with different Yb_2SiO_5/$Yb_2Si_2O_7$ (YbMS/YbDS) ratios were produced by modifying the plasma spraying parameters, and their microstructure, coefficient of thermal expansion (CTE), and elastic modulus were characterized. Cyclic steam exposures at 1350 °C were performed to assess the oxidation resistance.

The results showed that the EBC with a higher concentration of the Yb_2SiO_5 secondary phase exhibited a higher CTE, which is typically expected to shorten adhesion lifetime owing to the increased stress generated upon thermal cycling [91]. The multilayer EBC system (Si bonding layer + rare-earth silicate intermediate layer + glassy sealing layer) developed by GE Global Research Center achieved stable protection for over 500 h under conditions of 1400 °C/90% H_2O [92]. Self-healing environmental barrier coatings (EBCs) have been proposed to suppress crack damage induced by thermal cycling: crack-healing agents incorporated into the coating system—such as glass-forming silicide or boride phases, which oxidize to generate mobile silica- or borosilicate-glass, or low-melting SiO_2-containing secondary phases—flow into micro-cracks during high-temperature exposure and seal them. For example, cracks in mullite-based EBCs were healed via melting of a SiO_2-containing phase after 3000 thermal shock cycles [93].

Rare-earth silicate coating systems have been extensively evaluated for environmental barrier coating (EBC) applications. Meanwhile, the thermochemical stability of $RE_2Si_2O_7$ (RE = Sc, Nd, Er, Yb, or Lu) was experimentally investigated in high-temperature high-velocity steam (up to 235 m/s) at 1400 °C for 125 h; the water vapor reaction products, mass losses, and average reaction depths varied markedly among the different rare-earth disilicates, demonstrating that the choice of rare-earth element strongly governs the steam durability of the silicates [94]. Rejasse et al. (CNRS, France) fabricated a multilayer environmental barrier coating system consisting of a Si bond coat, a mullite interlayer, and a Yb_2SiO_5 topcoat via plasma spraying, and evaluated its oxidation protection performance for SiC substrates under high-temperature water-vapor exposure. The system was reported to substantially reduce the oxidation rate of SiC, although the specific quantitative claim of "an order of magnitude" reduction should be verified against the original experimental data [95].

In summary, coating design must holistically account for thermal expansion compatibility, chemical compatibility, radiative properties, and process feasibility. Multilayer composite coatings currently represent the most effective protection strategy. Coating effectiveness should be assessed under specific service atmospheres. Reducing environment from hydrogen combustion and high-oxidizing water-vapor-rich atmosphere from ammonia combustion put forward distinct requirements for substrate materials and protective coatings.

6. Material-Specific Considerations for Extreme Service Conditions of Hydrogen- and Ammonia-Fuel Combustion

6.1. Challenges Imposed by Hydrogen Combustion on Materials

Hydrogen exhibits an exceptionally high flame propagation velocity (~3 m/s), rendering it highly susceptible to flashback, and its adiabatic flame temperature can exceed 2100 °C, imposing more severe thermal shock demands on porous materials. These conditions necessitate materials with high thermal conductivity (for rapid temperature field homogenization), low thermal expansion, and a high thermal shock resistance parameter [21]. SiC and intermetallic compounds (Ni–Al) exhibit favorable behavior in this respect. Ni–Al porous burners have achieved a turndown ratio exceeding 13.8 at an equivalence ratio of 0.25 [96], demonstrating favorable anti-flashback behavior.

In the field of hydrogen-air combustion in porous media, previous studies have systematically examined the combustion characteristics of premixed gases in porous media of different ceramic materials. A mini-scale porous media combustor employing OB-SiC, Al_2O_3 and ZrO_2 porous matrices achieved stable hydrogen combustion across different equivalence ratios and thermal loads, with the hydrogen conversion rate and NO emission governed by the flame position and thermal load [97]. In porous media combustion, flashback (upstream flame propagation) occurs when the flame speed exceeds the mixture velocity, and its control is a key issue for porous burner design. Numerical investigations of modular porous burners with annular heat recirculation have examined the effect of porous media arrangement on combustion wave

propagation, flashback and start-up behavior [98]; for hydrogen-enriched fuels, dedicated flashback identification methods have further been proposed to clarify the boundary-layer flashback mechanism. Regarding the modeling of hydrogen combustion in porous media, two-dimensional numerical models with solid/gas energy equations, non-gray radiation transport and detailed chemical kinetics (e.g., GRI-Mech series) have been employed to predict flame stability, lean limits and emissions; e.g., the lean limit of methane was extended from $\varphi = 0.52$ (free flame) to $\varphi = 0.33$ in a porous medium flame and further to $\varphi = 0.26$ with hydrogen addition. Beyond porous media, large-eddy simulations with tabulated chemistry have been used to study high-pressure hydrogen jet combustion and NOx formation [99].

6.2. High-Temperature Water-Vapor Corrosion in Ammonia Combustion

Ammonia combustion generates substantial quantities of water vapor (~20–30%), which intensifies the oxidation of SiC [100]. Mullite-ytterbium silicate bilayer coatings have been validated as effective in resisting such corrosion, extending the service life of SiC skeletons by several-fold [31]. Furthermore, the fuel-bound NO_x generated during ammonia combustion cannot be eliminated through thermal management alone, necessitating the incorporation of catalytic functionality. Domestic researchers have proposed loading ammonia decomposition catalysts onto the first layer and NO_x decomposition catalysts onto the second layer of a dual-layer porous medium, thereby achieving catalytic-refractory integration—representing an emerging direction for multifunctional materials [101].

The Specchia group at Politecnico di Torino was among the first to explore the concept of a "catalytic porous burner", in which $LaMnO_3$ perovskite catalysts were deposited onto an industrial ceramic foam support by in situ pyrolysis, either as a thin surface layer on the burner deck or throughout the entire foam matrix. In pilot-scale tests (≈30 kW, 1600 kW/m^2), all burners achieved NO_x below 70 ppmv and unburned hydrocarbons below 10 ppmv; the catalysed versions, however, produced markedly less CO than the non-catalysed reference at low superficial power (<300 kW/m^2) and low excess air (<10%), and the catalyst also stabilised combustion at lower excess air, improving thermal efficiency [102]. Zhang, Zhou, Du et al. Conducted combustion experiments with CH_4/NH_3 and pure NH_3 in porous medium burners (PMB). By employing spatially resolved gas sampling within the porous structure, they elucidated the kinetics of NH_3 oxidation and NO_x formation. The use of staged combustion with 20–25% secondary air reduced NO_x emissions by 82.5%, resulted in unburned NH_3 levels below 20 ppm, and rendered N_2O undetectable [103].

6.3. Material-Structure Adaptability for Hydrogen-Ammonia Co-Combustion

Hydrogen-ammonia blending enables tunable reactivity; however, elevated hydrogen fractions introduce the coexistence of flashback risk and NO_x surges (reaching up to 12,607 ppm under certain operating conditions) [104]. From a structural design perspective, gradient porosity and TPMS configurations can simultaneously satisfy the requirements of upstream flashback prevention (small pore diameter) and downstream low-resistance combustion (large pore diameter) [105]. From a materials perspective, there is a need to develop composite ceramics capable of withstanding alternating oxidizing/reducing atmospheres, such as Si_3N_4/SiC or coating-protected SiC [61].

The research groups led by Hayakawa and Kobayashi at Tohoku University, Japan, have conducted extensive experimental studies on ammonia-hydrogen-air premixed swirling combustion, systematically elucidating the mechanism of fuel-derived NO_x formation in ammonia combustion and demonstrating the feasibility of achieving ultra-low emissions through staged combustion strategies [62,106]. The research team led by Valera-Medina at Cardiff University, United Kingdom, stands as one of the pioneers in global ammonia combustion research; they systematically evaluated the combustion stability and emission characteristics of NH_3/H_2 and NH_3/CH_4 mixed fuels under industrial gas turbine operating conditions, and proposed the concept of "ammonia cracking catalytic combustion"—in which a catalytic cracking layer is

prepositioned upstream of the burner to partially decompose NH_3 into N_2 and H_2 prior to combustion, thereby simultaneously enhancing combustion stability and suppressing NO_x formation [13]. Min and Yoo from the Korea Advanced Institute of Science and Technology (KAIST), South Korea, employed chemical kinetic analysis to reveal that when the volume fraction of H_2 in the NH_3/H_2 mixed fuel exceeds 30%, the flame propagation speed increases sharply, leading to flashback risks and elevated NO_x peak emissions; these findings provide critical input parameters for optimizing the hydrogen-ammonia fuel ratio in porous medium burners [38].

6.4. Fuel-Material-Structure Synergistic Selection Matrix

Based on the systematic review of intrinsic material properties (Section 3), topological thermomechanical responses (Section 4), and protective coatings (Section 6), Table 5 presents a synergistic "material-topology-protection" selection guideline for porous media tailored to different carbon-free fuels, serving as a bridge from fundamental understanding to engineering decision-making.

Table 5. Service-oriented fuel-material-topology-protection synergistic selection matrix under H_2, NH_3 and H_2/NH_3 blended combustion conditions.

Fuel Type	Core Service Challenges	Recommended Base Material	Recommended Topological Structure	Key Protection/Modification Strategies
H_2	Flashback, adiabatic flame temperature >2100 °C, high-frequency thermal cycling	High-thermal-conductivity SiC, Ni–Al intermetallic compounds	Upstream small-pore high-PPI gradient layer + downstream diamond lattice	High-density oxidation-resistant coating at the inlet section; integral thermal expansion matching design to reduce cyclic thermal stress [107]
NH_3	High water-vapor partial pressure (~20–30%), fuel-bound NO_x persistence, poor flame stability	Coating-protected SiC, mullite-based ceramics	Dual-/triple-layer axial gradient, with flame anchoring at interlayer interfaces [108]	Mullite-Yb_2SiO_5 or Al_2O_3-Cr_2O_3 bilayer coatings for hydrothermal corrosion resistance; second layer loaded with NO_x decomposition catalysts
H_2/NH_3 blend	Alternating oxidizing/reducing atmospheres, synergistic thermal and fuel-bound NO_x generation, combustion instability	Si_3N_4/SiC composite ceramics, ZTA-toughened ceramics	Topologically graded structures	Multilayer composite gradient coatings; integral catalytic functionalization [109]

The collaborative selection matrix proposed in this review follows a complete and cascading technical logic for porous media design and application. Variations in fuel combustion characteristics define the dominant service environments and corresponding material failure modes of porous skeletons. Hydrogen combustion mainly induces frequent cyclic thermal shock and potential flame flashback risks, while ammonia combustion generates high partial pressure water vapor, triggering severe hydrothermal corrosion and persistent nitrogen oxide emissions. These differentiated failure characteristics further determine the core protection priorities for porous components under different fuel conditions. For hydrogen-fueled service scenarios, material and structural optimization primarily focuses on improving thermal conductivity and achieving precise thermal expansion matching to alleviate cyclic thermal stress concentration. In contrast, ammonia combustion environments require dense, intact anti-oxidation coatings to block water vapor penetration and inhibit substrate hydrothermal degradation. The targeted protection requirements ultimately constrain the rational selection of substrate materials and the feasible design range of porous topological structures (Table 5).

In practical engineering applications, silicon carbide possesses excellent comprehensive thermophysical properties for high-temperature service, yet it cannot maintain long-term structural stability under ammonia combustion conditions without effective coating protection. Therefore, coated SiC is a preferred candidate for ammonia-fueled systems, subject to long-term validation of coating durability. For

hydrogen combustion systems with inherent flashback hazards, the upstream pore size of porous skeletons must be controlled below the flame quenching diameter to ensure combustion safety. This design principle limits the application of traditional uniform large-pore foam structures and guides the adoption of gradient porous architectures and triply periodic minimal surface configurations. Diamond-type topological structures with precise local pore size regulation capability exhibit favorable adaptability and stability, providing reliable structural optimization schemes for practical porous media design [110].

In the realm of standardization, the European Committee for Standardization (CEN) and the American Society for Testing and Materials (ASTM) have initiated the development of test methods for thermal shock of high-temperature porous ceramics and accelerated steam corrosion test protocols [111]. In multi-scale simulation, machine-learning-based surrogate models have recently been coupled with high-fidelity simulations of turbulent combustion: automated machine-learning-assisted frameworks have been developed to construct chemical reactor network surrogates for the Sandia turbulent methane/air flame, and Fourier neural operator surrogates have been employed for uncertainty quantification of Sandia/ETH jet flame simulations [112]. Meanwhile, Forschungszentrum Jülich (Germany) has established integrated multi-scale modeling frameworks for porous solid oxide fuel cell electrodes, spanning electrode microstructure reconstruction, cell and stack models, and system-level simulation [113]. Such multiscale electrode-modeling methodologies are, in principle, transferable to the simulation-aided design of porous burners, although this adaptation remains to be explored.

7. Summary and Future Research Perspectives

7.1. Research Summary

Unlike existing reviews focused on combustion regulation, flame stability, and flow-field design, this review establishes a full-chain logical relationship covering material intrinsic thermophysical properties, topological thermomechanical response, manufacturing-induced defects, service degradation mechanisms, and protective strategies, forming a complete material-oriented research system for hydrogen-ammonia combustion porous media. This review quantitatively constructs the internal correlation between material thermophysical parameters, internal thermal stress distribution, and macroscopic thermal shock failure based on the thermal shock resistance figure-of-merit.

(1) The ordered topological structure design can endow silicon carbide materials with a more significant thermal shock performance improvement effect compared with alumina materials, which provides reliable theoretical basis for the matching design of high-performance substrate materials and porous topological architectures.
(2) The coupled oxidation-volatilization failure mechanism of silicon carbide substrates within high-water-vapor environments produced by ammonia combustion is clarified, alongside a systematic collation of interfacial compatibility characteristics and practical protection performance for multiple coating systems: mullite, cordierite, alumina-chromia solid-solution, and rare-earth silicate coatings.
(3) Reasonable coating modification can substantially improve the residual strength (reported values: strength retention rising from 27% for uncoated substrates to up to 93.5% in laboratory-scale specimens). The core design principle of high-temperature protective coatings is to balance dense oxygen and water vapor barrier performance and thermal expansion compatibility with the substrate, so as to avoid interfacial cracking and failure under long-term thermal cycling.

On this basis, this review proposes a collaborative material-structure-coating selection system applicable to hydrogen, ammonia, and their blended zero-carbon fuels. The system forms a closed-loop design logic that takes fuel service characteristics as the initial boundary condition, defines dominant material failure modes under different combustion environments, determines targeted protection priorities, and further constrains the matching principles of substrate materials and porous topological structures,

providing practical and actionable theoretical references for the engineering design and performance optimization of high-temperature porous media components. Figure 10 provides a comprehensive summary of the structure and interrelationships of the main contents of this paper.

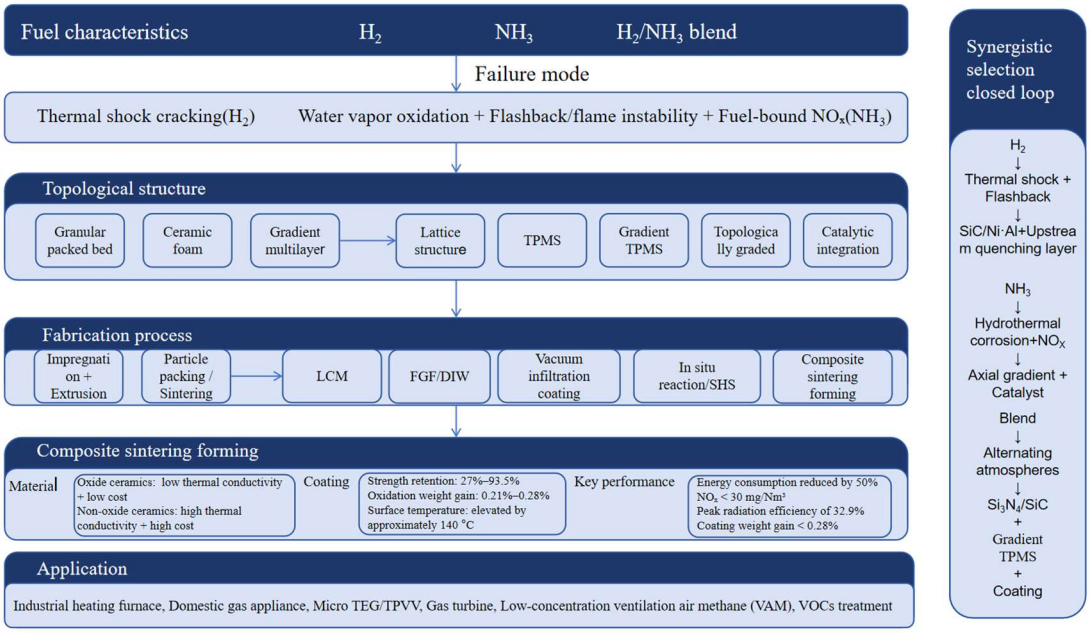


Figure 10. Full-chain correlation diagram of structure-process-performance-application relationships.

7.2. Future Perspectives

Future research on high-temperature porous media for H_2/NH_3 combustion can be organized into six interconnected, practically constrained research directions with quantifiable performance targets.

Values quoted below are marked as either [Literature anchored value], *i.e.*, experimentally measured data reported in the surveyed literature with the corresponding source given in brackets, or [Proposed prospective target (no unified experimental benchmark available)], *i.e.*, engineering thresholds proposed by the present review for benchmarking purposes. The latter are not derived from a unified experimental database and should be validated by round-robin testing before adoption as acceptance criteria.

7.2.1. Multiphase Composite and Gradient Material Design

Single-phase porous ceramics suffer inherent limitations under alternating extreme combustion environments: SiC features high thermal conductivity but is susceptible to hydrothermal volatilization in steam-rich NH_3 combustion; Si_3N_4 exhibits superior oxidation resistance but lower thermal conductivity. Multiphase composites (SiC–Si_3N_4, ZTA) and functionally graded architectures can balance these properties, yet material design is constrained by phase compatibility, CTE mismatch, and high-temperature degradation kinetics.

Si_3N_4/SiC composite porous ceramics: compressive strength of 62.4 MPa and fracture toughness of 4.8 MPa·m^(1/2) at 1200 °C with 69.3% porosity, retaining approximately 91% of their strength after 100 thermal cycles—[Literature anchored value] (Section 2.2).

Gradient pore design extends thermal cycling life by 2–3 times relative to a uniform pore structure—[Literature anchored value] (Section 3.2, [58]).

Strength retention ≥60% after 100 thermal cycles (RT ↔ 1000 °C) as the minimum target, and ≥70% after 500 cycles (RT ↔ 1200 °C) as the aspirational target—[Proposed prospective target (no unified experimental benchmark available)].

Mass loss below 5% after 500 h isothermal exposure at 1200 °C in 20% H_2O, and below 3% after 500 h at 1300 °C in 30% H_2O (Table 6)—[Proposed prospective target (no unified experimental benchmark available)]; the water-vapor contents of 20–30% correspond to ammonia combustion atmospheres (Section 6.2, [21]).

Table 6. The Performance Benchmark Table.

Performance Parameter	Minimum Target	Aspirational Target	Rationale
Service temperature limit	1200 °C continuous	1400 °C continuous	Upper range of porous media combustion operating window
Thermal shock durability	>100 cycles, RT ↔ 1000 °C, >60% strength retention	>500 cycles, RT ↔ 1200 °C, >70% strength retention	Typical burner start–stop frequency and thermal amplitude
Hydrothermal corrosion resistance	<5% weight loss after 500 h at 1200 °C, 20% H_2O	<3% weight loss after 500 h at 1300 °C, 30% H_2O	Representative ammonia combustion conditions
Compressive strength at service temperature	>1 MPa at 1200 °C with >65% porosity	>2 MPa at 1400 °C with >65% porosity	Minimum structural integrity for self-supporting porous elements
Pressure drop coefficient	<500 Pa at face velocity 0.5 m/s (porosity 70–80%)	<200 Pa at face velocity 0.5 m/s	Combustion efficiency requires low flow resistance
Coating adhesion (ASTM C633 adapted)	>15 MPa at RT, >10 MPa after 50 thermal cycles	>25 MPa at RT, >15 MPa after 100 thermal cycles	Preventing coating spallation under service conditions
Infrared emissivity of coating	>0.75 (proposed)	>0.85 (anchor: cordierite ≈0.85–0.9, Section 5.2)	Radiative output efficiency
Coating service life	no visible spallation after 500 h at 1300 °C (proposed)	no visible spallation after 1000 h at 1300 °C (proposed)	Long-duration ammonia combustion exposure

7.2.2. Multifunctional Gradient Protective Coatings

Single-layer coatings cannot simultaneously satisfy CTE matching, hydrothermal barrier performance and long-term thermal cycling stability. Gradient composite coatings combining dense barrier layers, high-emissivity outer layers and self-healing interlayers represent a promising route.

Mullite coatings raised the residual strength retention of SiC from 27% (uncoated) to 93.5%—[Literature anchored value] (Section 5.1, [25]).

Cordierite–SiC–cordierite three-layer architecture: residual strength retention of 67% and compressive strength of 1.18 MPa after thermal treatment at 1350 °C; burner surface temperature elevated by ≈140 °C—[Literature anchored value] (Sections 2.3 and 5.2, [71]).

Al_2O_3–Cr_2O_3 solid-solution coating: oxidation weight gain of merely 0.21–0.28% after 100 h at 1500 °C, with no appreciable delamination—[Literature anchored value] (Sections 2.1 and 5.3).

Multilayer EBC (Si bonding layer + rare-earth silicate intermediate layer + glassy sealing layer): stable protection for over 500 h at 1400 °C/90% H_2O—[Literature anchored value] (Section 5.4, [29]).

$Yb_2Si_2O_5$/mullite double-layer coatings reduce the oxidation rate of SiC substrates by one order of magnitude at 1200 °C/50% H_2O—[Literature anchored value] (Section 5.4, [32]).

Infrared emissivity: 0.262→0.588 (micro-silica modified Al_2O_3) and 0.52→0.71 (flower-like CeO_2)—[Literature anchored value] (Section 2.1); ≈0.8509 (cordierite) and ≈0.9 (cordierite coating)—[Literature anchored value] (Sections 2.3 and 5.2).

Residual strength retention ≥80% after 200 thermal cycles—[Proposed prospective target (no unified experimental benchmark available)].

No visible spallation after 1000 h exposure at 1300 °C (Table 6)—[Proposed prospective target (no unified experimental benchmark available)].

Sustained infrared emissivity above 0.75—[Proposed prospective target (no unified experimental benchmark available)], selected as an intermediate value between the measured ranges of 0.52→0.71 and ≈0.85–0.9.

Uniform coating deposition inside high-porosity interconnected skeletons remains a major challenge (Figure 7) [20,24].

7.2.3. Low-Defect Ceramic Additive Manufacturing

Additive manufacturing enables complex TPMS/lattice topologies inaccessible via conventional routes, though complete elimination of structural defects is unrealistic. Key bottlenecks include binder burnout kinetics, anisotropic sintering shrinkage, interlayer delamination, and anisotropic mechanical weakness along the printing direction.

LCM (Lithoz): layer-thickness precision of up to 25 μm and density exceeding 99% of the theoretical density—[Literature anchored value] (Section 4.2, [45]).

CeraMax series (3DCeram-Sinto): fabrication of large-sized ceramic components up to 410 × 410 × 200 mm—[Literature anchored value] (Section 4.2, [46]).

Optimized degreasing/heating profiles with microwave-assisted sintering: residual porosity of additively manufactured SiC reduced from approximately 12% to below 3%—[Literature anchored value] (Section 4.2, [50]).

Geometric fidelity within ±5% of the designed strut thickness—[Proposed prospective target (no unified experimental benchmark available)]; the surveyed literature only quantifies layer-thickness precision (≈25 μm), which is not equivalent to strut-thickness fidelity.

More than 75% strength retention after 100 thermal cycles—[Proposed prospective target (no unified experimental benchmark available)].

Reduction of production cost to less than three times that of conventional routes within five years—[Proposed prospective target (no unified experimental benchmark available)] (roadmap statement, not a performance criterion).

7.2.4. Integration of Refractory Skeleton and Catalytic Modification

Combining structural refractory performance with *in-situ* NO_x purification creates a multifunctional substrate, yet critical technical barriers must be acknowledged: catalytic nanoparticles sinter rapidly at 900–1500 °C; local hotspots from exothermic reactions induce thermal strain and coating spallation due to CTE mismatch; catalyst zoning must match the burner's inherent temperature gradient without sacrificing porosity or flow resistance.

Rh-loaded SiC foam enabling *in-situ* catalytic decomposition and combustion of NH_3: fuel-derived NO_x emissions reduced by approximately 60%—[Literature anchored value] (Section 6.2, [98]).

Perovskite catalysts ($LaCoO_3$, $LaMnO_3$) loaded on porous SiC skeletons: stable methane combustion under ultra-lean conditions with CO emissions below 5 ppm—[Literature anchored value] (Section 6.2, [97]).

SiC porous combustors sustaining stable combustion at $\varphi = 0.3$ with NO_x emissions remaining below 10 ppm—[Literature anchored value] (Section 6.1, [93]).

Over 70% catalytic activity retention after 100 h at 800 °C—[Proposed prospective target (no unified experimental benchmark available)].

NO_x reduction efficiency exceeding 50%—[Proposed prospective target (no unified experimental benchmark available)], set below the measured ≈60% reduction over Rh-loaded SiC foam.

Additional pressure drop below 10% relative to non-catalytic porous structures of identical geometry; the absolute criterion of Table 6 (<500 Pa at a face velocity of 0.5 m/s with 70–80% porosity) should be

reported in parallel—[Proposed prospective target (no unified experimental benchmark available)]; no quantitative pressure-drop data for catalytic porous structures were reported in the surveyed literature.

7.2.5. Multi-Scale Simulation and Inverse Design

Multiscale modeling coupled with *in-situ* high-temperature characterization accelerates material screening, yet data scarcity imposes fundamental limitations. High-temperature thermomechanical, corrosion, and thermal fatigue datasets are sparse and non-standardized, which risks overfitting for purely data-driven machine learning models. Reliable predictions require temperature-dependent constitutive models that capture creep, cyclic damage, and oxidation-induced strut thinning. Machine learning is most suitable for fast parameter screening and surrogate modeling, rather than extrapolation far outside the training domain.

Coupled DNS + machine-learning surrogate models for turbulent combustion and thermal stress in porous media—[Literature anchored value] (methodology, Section 6.4, [107]).

Multi-scale modeling framework for porous electrode structures adaptable to porous combustor design—[Literature anchored value] (methodology, Section 6.4, [108]).

Two-dimensional model quantitatively predicting the scaling relationship between the flashback limit and pore diameter—[Literature anchored value] (methodology, Section 6.1, [94]).

Thermomechanical model prediction error below 15%, open benchmark datasets, and topology optimization within 24 h of computation—[Proposed prospective target (no unified experimental benchmark available)].

7.2.6. Standardized Testing Protocols and Performance Benchmarks

Unified testing protocols for porous combustor components and hydrothermal corrosion remain incomplete: the European Committee for Standardization (CEN) and the American Society for Testing and Materials (ASTM) have initiated the development of test methods for thermal shock of high-temperature porous ceramics and accelerated steam corrosion test protocols (Section 6.4, [63]; ASTM C1525-18[111]). Priority should be placed on standardized thermal shock and hydrothermal corrosion test protocols defining specimen geometry, thermal cycling profiles, and quantitative failure criteria such as strength retention and crack density. Full life-cycle carbon and economic assessment is valuable but should follow experimental benchmark validation rather than being pursued prematurely. Cross-disciplinary industrial collaboration is required to validate laboratory findings at burner scale.

A draft standard test protocol within two years, a shared benchmark database within three years, and continuous component validation exceeding 1000 h within five years—[Proposed prospective target (no unified experimental benchmark available)] (roadmap targets).

Statement of the Use of Generative AI and AI-Assisted Technologies in the Writing Process

During the writing process, we utilized the XIAOMI MIMO Studio and the The built-in DeepSeek model of the National Science and Technology Library and Documentation Center for reasoning and data collection.

Acknowledgments

The author sincerely thanks Pan Liping for her assistance in the manuscript layout and in the revision and supplementation of the content.

Author Contributions

C.M.: Writing—Original Draft, Investigation, Writing—Review & Editing, Data Curation. L.P.: Writing—Review & Editing, Supervision, Conceptualization. E.W.: Writing—Review & Editing,

Resources. C.L.: Writing—Review & Editing, Resources. Y.L.: Supervision, Writing—Review & Editing. X.L.: Writing—Review & Editing. Y.D.: Writing—Review & Editing. P.Z.: Writing—Review & Editing.

Ethics Statement

Not applicable.

Informed Consent Statement

Not applicable.

Data Availability Statement

Data will be made available on request.

Funding

This research received no external funding.

Declaration of Competing Interest

The authors declare that they have no known competing financial interests or personal relationships that could have appeared to influence the work reported in this paper.

References

1. Sasanpour S, Cao KK, Gils HC, Jochem P. Strategic policy targets and the contribution of hydrogen in a 100% renewable European power system. *Energy Rep*. **2021**, *7*, 4595−4608. DOI:10.1016/j.egyr.2021.07.005
2. Kurata O, Iki N, Matsunuma T, Inoue T, Tsujimura T, Furutani H, et al. Performances and emission characteristics of NH_3–air and NH_3–CH_4–air combustion gas turbine–generating power. *Proc. Combust. Inst*. **2017**, *36*, 3351−3359. DOI:10.1016/j.proci.2016.07.088
3. Mac Dowell N, Fennell PS, Shah N, Maitland GC. The role of CO_2 capture and utilization in mitigating climate change. *Nat. Clim. Change* **2017**, *7*, 243−249. DOI:10.1038/nclimate3231
4. Makaryan IA, Sedov IV, Munoz-Herrera C, Toledo M, Salgansky EA. Combustion of ammonia-blended fuels in porous media burners, with storage and distribution implications: A review. *Renew. Sustain. Energy Rev.* **2025**, *220*, 115884. DOI:10.1016/j.rser.2025.115884
5. Devi S, Sahoo N, Muthukumar P.Experimental studies on biogas combustion in a novel double layer inert Porous Radiant Burner. *Renew. Energy***2020**, *149*, 1040–1052. DOI:10.1016/j.renene.2019.10.092
6. Wood S, Harris AT. Porous burners for lean-burn applications. *Prog. Energy Combust. Sci*. **2008**, *34*, 667−684. DOI:10.1016/j.pecs.2008.04.003
7. Wang EY, Chen MM, Shi ZT, Tian L. Radiation Output Efficiency and CO Emissions in Modular Porous Media Burner. *J. Combust. Sci. Technol*. **2022**, *28*, 322−328. Available online: https://pubnr.napstic.cn/periodicalArticle/010rskxyjs202203012 (accessed on 21 October 2026).
8. Tolouei A, Gharehghani A. Numerical investigation of premixed methane-ammonia combustion in a mesoscale porous combustor. *Fuel*. **2024**, *366*, 131427. DOI:10.1016/j.fuel.2024.131427
9. Yang R, Chen YC, Deng YF, Sun SJ, Zhao WQ, Yang JH, et al. Effect of high temperature thermal exposure on properties of Al2O3/Al2O3 ceramic matrix composites. *J. Aeronaut. Mater*. **2023**, *43*, 1−8. DOI:10.11868/j.issn.1005-5053.2023.000006
10. Liang X, Li Y, He Z, Wang Q, Chen Y, Xu X, et al. Design of three-layered struts in SiC reticulated porous ceramics for porous burner. *Ceram. Int*. **2019**, *45*, 8571−8576. DOI:10.1016/j.ceramint.2019.01.175
11. More KL, Tortorelli PF, Walker LR. Effects of high water vapor pressures on the oxidation of SiC-Based fiber-reinforced composites. *Mater. Sci. Forum*. **2001**, *369−372*, 385−393. DOI:10.4028/www.scientific.net/msf.369-372.385
12. Chen H, Pan X, Gao Y, Shi J, Xu X, Huo X. Interpretation on the PRISMA Statement Extension for Living Systematic Review (PRISMA-LSR). *Med. J. Peking Union Med. Coll. Hosp*. **2025**, *16*, 1563−1570. DOI:10.12290/xhyxzz.2024-1064

13. Muto D, Hashimoto S, Daiko Y, Honda S, Iwamoto Y. Characteristics of castables incorporating highly porous alumina aggregates fabricated by high-temperature evaporation method. *Ceram. Int.* **2019**, *45*, 13509−13517. DOI:10.1016/j.ceramint.2019.04.055
14. Zake-Tiluga I, Svinka V, Svinka R, Grase, Liga. Thermal shock resistance of porous Al_2O_3-mullite ceramics. *Ceram. Int.* **2015**, *41*, 11504–11509. DOI:10.1016/j.ceramint.2015.05.116
15. Qiao W, Nie J, Qiu W, Wang L, Liang Y, Yin Y, et al. The influence of silica powder on the properties of Al_2O_3-SiC-C molding sand combined with silica sol. *Refractories* **2014**, *48*, 331–334. DOI:10.3969/j.issn.1001-1935.2014.05.003
16. Li P, Sun H, Li J, Yan S, Wang G, Du Y. Effect of fused zirconia mullite on thermal shock resistance of Al_2O_3-Cr_2O_3 refractories. *Refractories* **2017**, *51*, 250–255. Available online: http://www.nhcl.cn/CN/Y2017/V51/I4/250 (accessed on 21 October 2026).
17. Dong B, Yu C, Deng C, Zhu H, Ding J, Zhu Q. Research Progress on the High-Temperature Properties of Reactively Sintered Silicon Carbide. *Refractories* **2022**, *56*, 75–81. DOI:10.3969/j.issn.1001-1935.2022.01.017
18. Chávez-Valdez A, Almanza-Robles JM, Vargas-Gutiérrez G, Arizmendi-Morquecho A. Adhesion strength and thermal shock resistance of fly ash cenospheres deposited on SiC. *Mater. Charact.* **2010**, *61*, 1299–1303. DOI:10.1016/j.matchar.2010.09.003
19. Zhou P, Fan Y, Wang P, Chen J. The indentation thermal shock behavior of laminated ZrB_2-SiC ceramics with strong interfaces. *Ceram. Int.* **2016**, *42*, 17489–17496. DOI:10.1016/j.ceramint.2016.08.056
20. Eckel ZC, Zhou C, Martin JH, Jacobsen AJ, Carter WB, Schaedler TA. Additive manufacturing of polymer-derived ceramics. *Science* **2016**, *351*, 58–62. DOI:10.1126/science.aad2688
21. Vance FH, de Goey LPH, van Oijen JA. Development of a flashback correlation for burner-stabilized hydrogen-air premixed flames. *Combust. Flame* **2022**, *243*, 112045. DOI:10.1016/j.combustflame.2022.112045
22. Valera-Medina A, Xiao H, Owen-Jones M, David WIF, Bowen PJ. Ammonia for power. *Prog. Energy Combust. Sci.* **2018**, *69*, 63–102. DOI:10.1016/j.pecs.2018.07.001
23. Li J, Deng Z, Tu X, Chen Y. Preparation methods of porous ceramics and their applications. *J. Ceram.* **2017**, *38*, 138–143. DOI:10.13957/j.cnki.tcxb.2017.02.002
24. Sobhani S, Allan S, Muhunthan P, Boigne E, Ihme M. Additive manufacturing of tailored macroporous ceramic structures for high-temperature applications. *Adv. Eng. Mater.* **2020**, *22*, 2000158. DOI:10.1002/adem.202000158
25. Zhang K, Meng Q, Qu Z, He R. From defect control to mechanical enhancement: A pathway via X-ray computed tomography for vat photopolymerization additive manufactured Al_2O_3 ceramics. *J. Alloys Compd.* **2026**, *1059*, 187209. DOI:10.1016/j.jallcom.2026.187209
26. Yang H, Zhou X, Yu J, Wang H, Huang Z. Microwave and conventional sintering of the SiC/SiC composites: The densification and pore distributions. *J. Alloys Compd.* **2016**, *662*, 252–258. DOI:10.1016/j.jallcom.2015.12.085
27. Vishwanath N, Suryakumar S. Use of fractal curves for reducing spatial thermal gradients and distortion control. *J. Manuf. Process.* **2022**, *81*, 594–604. DOI:10.1016/j.jmapro.2022.07.028
28. Li G, Qin L, Cao X, Lu X, Tu Y, Zhang H, et al. Water vapor corrosion resistance and failure mechanism of SiCf/SiC composites completely coated with plasma sprayed tri-layer EBCs. *Ceram. Int.* **2022**, *48*, 7082–7092. DOI:10.1016/j.ceramint.2021.11.267
29. Reddy NK. Properties of silicate-bonded silicon carbide refractories. *Mater. Lett.* **2001**, *47*, 305–307. DOI:10.1016/s0167-577x(00)00254-8
30. Wang Y, Wang W, Cao X, Zhang Z, Li J, Han G, et al. Failure behavior of SiC/SiC composites with Si/Yb_2SiO_5 and Si/mullite/Yb_2SiO_5 EBCs in wet oxygen at 1350 °C. *Int. J. Appl. Ceram. Technol.* **2024**, *21*, 358–369. DOI:10.1111/ijac.14491
31. Han M, Xue W, Sun J. The Effect of Adding SiC on the Valence State of Chromium in the Aluminum-Chromium System at High Temperatures. *Refractories* **2008**, *42*, 109–112. DOI:10.3969/j.issn.1001-1935.2008.02.006
32. Valaskova M, Koci K, Kupkova J. Cordierite/steatite/CeO_2 porous materials—Preparation, structural characterization and their photocatalytic activity. *Microporous Mesoporous Mater.* **2015**, *207*, 120–125. DOI:10.1016/j.micromeso.2014.12.035
33. Mujeebu MA, Abdullah MZ, Bakar MZA, Mohamad AA, Abdullah MK. A review of investigations on liquid fuel combustion in porous inert media. *Prog. Energy Combust. Sci.* **2009**, *35*, 216–230. DOI:10.1016/j.pecs.2008.11.001
34. Cao H, Wang W, Zhang X, Xu H, Li J. High-temperature oxidation behavior of silicon carbide molding materials in air and steam at 1000°C. *Refractories* **2022**, *56*, 16–19. Available online: http://www.nhcl.cn/CN/Y2022/V56/I1/16 (accessed on 21 October 2026).
35. Cao H, Wu J, Cheng Z, Li J, Huang Z. The influence of B_4C on the thermal shock resistance of Si_3N_4/Si_2N_2O-bonded SiC materials. *Refractories* **2023**, *57*, 70–73. DOI:10.3969/j.issn.1001-1935.2023.01.015

36. Droschel M, Hoffmann MJ, Oberacker R. SiC-Ceramics with Tailored Porosity Gradients for Combustion Chambers. *Key Eng. Mater.* **2000**, *175–176*, 149–162. DOI:10.4028/www.scientific.net/kem.175-176.149
37. Boyarchenko OD, Sychev AE, Umarov LM, Shchukin AS, Kovalev ID, Sichinava MA. Structure and Properties of a Composite Material Obtained by Thermal Explosion in a Mixture of Ni + Al + Cr_2O_3. *Combust. Explos. Shock Waves* **2017**, *53*, 41–48. DOI:10.1134/s0010508217010075
38. Li S, Si TY, Liang KC, Zhang H, Cheng ZL, Wang QW. Numerical Study of Heat and Mass Transfer in Reactive Flow Based on Customized Porous Media. *Chin. J. Eng. Thermophys.* **2023**, *44*, 2849–2854. Available online: https://scholar.xjtu.edu.cn/en/publications/%E5%9F%BA%E4%BA%8E%E5%AE%9A%E5%88%B6%E5%AD%94%E9%9A%99%E7%9A%84%E5%A4%9A%E5%AD%94%E4%BB%8B%E8%B4%A8%E5%8F%8D%E5%BA%94%E6%B5%81%E7%83%AD%E8%B4%A8%E4%BC%A0%E9%80%92%E7%A0%94%E7%A9%B6/ (accessed on 21 October 2026).
39. Wang S, Jiang Y, Hu J, Fan X, Luo Z, Liu Y, et al. Efficient representation and optimization of TPMS-based porous structures for 3D heat dissipation. *Comput.-Aided Des.* **2022**, *142*, 103123. DOI:10.1016/j.cad.2021.103123
40. Gao HB, Qu ZG, Feng XB, Tao WQ. Methane/air premixed combustion in a two-layer porous burner with different foam materials. *Fuel* **2014**, *115*, 154–161. DOI:10.1016/j.fuel.2013.06.023
41. Sankineni R, Ravi Kumar Y. Evaluation of energy absorption capabilities and mechanical properties in FDM printed PLA TPMS structures. *Proc. Inst. Mech. Eng. Part C J. Mech. Eng. Sci.* **2022**, *236*, 3558–3577. DOI:10.1177/09544062211039530
42. Meng Q, Zhang K, Yang S, He R, Qu Z. Thermal shock resistance study of stereolithographic additive-manufactured Al_2O_3 ceramics by in situ digital radiography. *Ceram. Int.* **2022**, *48*, 30086–30092. DOI:10.1016/j.ceramint.2022.06.279
43. Cheng Z, Xu R, Jiang PX. Morphology, flow and heat transfer in triply periodic minimal surface based porous structures. *Int. J. Heat Mass Transf.* **2021**, *170*, 120902. DOI:10.1016/j.ijheatmasstransfer.2021.120902
44. Bhat C, Kumar A, Jeng JY. Effect of atomic tessellations on structural and functional properties of additive manufactured lattice structures. *Addit. Manuf.* **2021**, *47*, 102326. DOI:10.1016/j.addma.2021.102326
45. Peng Z, Wang Y, Yang L, Fan Z. Research on the Accuracy of Three-Head Extrusion Formed Alumina-Based Ceramics. *China Mech. Eng.* **2024**, *35*, 481–486. DOI:10.3969/j.issn.1004-132x.2024.03.010
46. Yu D, Zhang X, Wu N, Liao H. The influence of granulation particle size distribution on the porosity of ZrO_2 ceramic bearing bodies. *Refractories* **2020**, *54*, 427–429. DOI:10.3969/j.issn.1001-1935.2020.05.013
47. Catchpole-Smith S, Selo RRJ, Davis AW, Ashcroft IA, Tuck CJ, Clare A. Thermal conductivity of TPMS lattice structures manufactured via laser powder bed fusion. *Addit. Manuf.* **2019**, *30*, 100846. DOI:10.1016/j.addma.2019.100846
48. Alhammadi A, Al-Ketan O, Khan KA, Ali M, Rowshan R, Abu Al-Rub RK. Microstructural characterization and thermomechanical behavior of additively manufactured AlSi10Mg sheet cellular materials. *Mater. Sci. Eng. A* **2020**, *791*, 139714. DOI:10.1016/j.msea.2020.139714
49. Pfeiffer S, Florio K, Puccio D, Grasso M, Colosimo BM, Aneziris CG, et al. Direct laser additive manufacturing of high performance oxide ceramics: A state-of-the-art review. *J. Eur. Ceram. Soc.* **2021**, *41*, 6087–6114. DOI:10.1016/j.jeurceramsoc.2021.05.035
50. Schwentenwein M, Homa J. Additive manufacturing of dense alumina ceramics. *Int. J. Appl. Ceram. Technol.* **2015**, *12*, 1–7. DOI:10.1111/ijac.12319
51. Lithoz. Ceramic 3D Printer: CeraMax Vario V900 [EB/OL]. [2026-11-01]. Available online: https://www.lithoz.com/en/3d-printer/ceramax-vario-v900/ (accessed on 30 July 2026).
52. Bedoya C, Dinkov I, Habisreuther P, Zarzalis N, Bockhorn H, Parthasarathy P. Experimental study, 1D volume-averaged calculations and 3D direct pore level simulations of the flame stabilization in porous inert media at elevated pressure. *Combust. Flame* **2015**, *162*, 3740–3754. DOI:10.1016/j.combustflame.2015.07.012
53. Zhang T, Tan Q, Feng Z, Wang H, Liu P. The influence of stabilizer types on the properties of high-purity zirconia hollow sphere products. *Refractories* **2023**, *57*, 397–401. DOI:10.3969/j.issn.1001-1935.2023.05.005
54. Samoilenko M, Seers P, Terriault P, Brailovski V. Design, manufacture and testing of porous materials with ordered and random porosity: Application to porous medium burners. *Appl. Therm. Eng.* **2019**, *158*, 113724. DOI:10.1016/j.applthermaleng.2019.113724
55. Jiao X, Liu Y, Cai X, Wang J, Feng P. Progress of porous Al-containing intermetallics fabricated by combustion synthesis reactions: A review. *J. Mater. Sci.* **2021**, *56*, 11605–11630. DOI:10.1007/s10853-021-06035-5
56. Al-Ketan O, Ali M, Khalil M, Rowshan R, Khan KA, Abu Al-Rub RK. Forced convection CFD analysis of architected and 3D printable heat sinks based on triply periodic minimal surfaces. *J. Therm. Sci. Eng. Appl.* **2021**, *13*, 021010. DOI:10.1115/1.4047385

57. Tang W, Zhou H, Zeng Y, Yan M, Jiang C, Yang P, et al. Analysis on the convective heat transfer process and performance evaluation of triply periodic minimal surface (TPMS) based on Diamond, Gyroid and Iwp. *Int. J. Heat Mass Transf.* **2023**, *201*, 123642. DOI:10.1016/j.ijheatmasstransfer.2022.123642
58. Liu J, Xue Q, Zhou Y, Qu Q. The Effects of Adding Li_2CO_3 and $BaCO_3$ on the Properties of Synthetic Pyrochlore. *Refractories* **2007**, *41*, 421–423. DOI:10.3969/j.issn.1001-1935.2007.06.006
59. Wang Y, Wu H, Jia B, Zhang Y, Zhang Z, Liu C, et al. Research Progress on Sintering Additives for High Thermal Conductivity Silicon Nitride Ceramics. *Powder Metall. Technol.* **2024**, *42*, 1–13. DOI:10.19591/j.cnki.cn11-1974/tf.2021070001
60. Bai GZ, Zhang YJ, Liu XY, Dai JJ, Wang XT, Zhang HL. High-temperature thermal conductivity and thermal cycling behavior of Cu-B/Diamond composites. *IEEE Trans. Compon. Packag. Manuf. Technol.* **2020**, *10*, 626–636. DOI:10.1109/tcpmt.2019.2958056
61. Li D, de Moraes EG, Colombo P, Shen Z. Preparation of nasal cavity-like SiC-Si_3N_4 foams with a hierarchical pore architecture. *RSC Adv.* **2015**, *5*, 27891–27900. DOI:10.1039/c5ra00766f
62. Khateeb AA, Guiberti TF, Zhu X, Younes M, Jamal A, Roberts WL. Stability limits and NO emissions of technically-premixed ammonia-hydrogen-nitrogen-air swirl flames. *Int. J. Hydrogen Energy* **2020**, *45*, 22008–22018. DOI:10.1016/j.ijhydene.2020.05.236
63. Osipova KN, Sarathy SM, Korobeinichev OP, Shmakov AG. Chemical structure of premixed ammonia/hydrogen flames at elevated pressures. *Combust. Flame* **2022**, *246*, 112419. DOI:10.1016/j.combustflame.2022.112419
64. Yin Z, Wang P, Jiang L, He Y, He Z. Experimental Study of Flame Characteristics in Simple Cubic Packed Beds. *J. Shanghai Jiao Tong Univ.* **2023**, *57*, 326–334. DOI:10.16183/j.cnki.jsjtu.2021.317
65. Zhao P, Ye T, Ding M, Chen Y, Liu M. Radiation Output Efficiency and Emissions in a Porous Burner. *J. Combust. Sci. Technol.* **2007**, *13*, 549–553. DOI:10.3321/j.issn:1006-8740.2007.06.013.
66. Yue M, Xie M, Shi J, Liu H. Experimental Study on Premixed Gas Combustion Characteristics in an Ordered Packing Bed. *J. Therm. Sci. Technol.* **2021**, *20*, 48–53. DOI:10.13738/j.issn.1671-8097.020222
67. Ahmed MI, Hibbert DB, Zhao C. Rational catalyst design and mechanistic evaluation for electrochemical nitrogen reduction at ambient conditions. *Green Energy Environ.* **2023**, *8*, 1567–1595. DOI:10.1016/j.gee.2022.10.001
68. Zuo C, Li Q, Wang Q, Li Y, Li L, Wei J, et al. Effect of material parameters on thermal shock crack of ceramics calculated by phase-field method. *J. Am. Ceram. Soc.* **2022**, *105*, 7649–7657. DOI:10.1111/jace.18720
69. Deckers J, Vleugels J, Kruth JP. Additive Manufacturing of Ceramics: A review. *J. Ceram. Sci. Technol.* **2014**, *5*, 245–260. DOI:10.4416/jcst2014-00032
70. Lei N, Wang W, Wan L, Wu J. Preparation and oxidation resistance of $MoSi_2$-SiC materials. *Refractories* **2018**, *52*, 365–367. DOI:10.3969/j.issn.1001-1935.2018.05.011
71. Rezaei E, Haussener S, Gianella S, Ortona A. Early-stage oxidation behavior at high temperatures of SiSiC cellular architectures in a porous burner. *Ceram. Int.* **2016**, *42*, 16255–16261. DOI:10.1016/j.ceramint.2016.07.159
72. Gaudillere C, Serra JM. Freeze-casting: Fabrication of highly porous and hierarchical ceramic supports for energy applications. *Bol. Soc. Esp. Ceram. Vidr.* **2016**, *55*, 45–54. DOI:10.1016/j.bsecv.2016.02.002
73. Miao Z, Li N, Yan W. Effects of Raw Material Ratio on the Microstructure and Properties of Calcium Feldspar-Morilite Composite Porous Ceramics. *Refractories* **2015**, *49*, 259–263. DOI:10.3969/j.issn.1001-1935.2015.04.005
74. Bai JG, Zhao J. The influence of mullite content on the properties of magnesia-carbonite-mullite composite ceramics. *Refractories* **2008**, *42*, 365–367. DOI:10.3969/j.issn.1001-1935.2008.05.012
75. Lao X, Xu X, Jiang W, Liang J, Miao L, Wu Q. Influences of impurities and mineralogical structure of different kaolin minerals on thermal properties of cordierite ceramics for high-temperature thermal storage. *Appl. Clay Sci.* **2020**, *187*, 105485. DOI:10.1016/j.clay.2020.105485
76. Ren Y, Yin H, Zhang J, Gao K, Li J. Preparation and Performance Study of Mollite-Titanate Alumina Kilnware. *Refractories* **2009**, *43*, 214–217. DOI:10.3969/j.issn.1001-1935.2009.03.014
77. Nan B, Cui W, Wu L, Jiang Y. Preparation of porous Ni_3Al by addition of ammonium carbonate. *Mater. Sci. Eng. Powder Metall.* **2014**, *19*, 622–627. Available online: https://lib.cqvip.com/Qikan/Article/Detail?id=662177397 (accessed on 21 October 2026).
78. Bewlay BP, Jackson MR, Zhao JC, Subramanian PR, Mendiratta MG, Lewandowski JJ. Ultrahigh-temperature Nb-silicide-based composites. *MRS Bull.* **2003**, *28*, 646–653. DOI:10.1557/mrs2003.192
79. Chen R, He D, Wang Y, Zhou Q, Liu X, Xiao Q, et al. Research Status of Porous Structural Ceramics Prepared by Organic Foam Impregnation Method. *Refractories* **2018**, *52*, 475–480. DOI:10.3969/j.issn.1001-1935.2018.06.018
80. Ceniga L. Thermal stresses in SiC-Si_3N_4 cubic-cell-divided multi-particle-matrix system. *Key Eng. Mater.* **2005**, *290*, 320–323. DOI:10.4028/www.scientific.net/kem.290.320

81. Li WG, Fang DN. Effects of thermal environments on the thermal shock resistance of Ultra-High Temperature Ceramics. *Mod. Phys. Lett. B* **2008**, *22*, 1375–1380. DOI:10.1142/s021798490801608x
82. Kim IS, Kim IG. Thermal shock behaviour of Al_2O_3-SiC composites made by directed melt oxidation of Al-alloy. *J. Mater. Sci. Lett.* **1997**, *16*, 772–775. DOI:10.1023/a:1018505819868
83. Wang Z, Ma S, Zhang L, Bu J. The influence of titanium dioxide content on the properties of Al_2O_3-Al_2TiO_5 composite materials. *Refractories* **2008**, *42*, 375–378. DOI:10.3969/j.issn.1001-1935.2008.05.015
84. Imariouane M, Saadaoui M, Denis G, Reveron H, Chevalier J. Low-yttria doped zirconia: Bridging the gap between strong and tough ceramics. *J. Eur. Ceram. Soc.* **2023**, *43*, 4906–4915. DOI:10.1016/j.jeurceramsoc.2023.04.021
85. Yan J, Zhang H, Li Y, Li S. Research Progress on Oxidation Behavior of Binary Silicide Molybdenum-Based High-Temperature Structural Materials. *Mater. Rep.* **2005**, *19*, 65–68. DOI:10.3321/j.issn:1005-023x.2005.11.018
86. Brenner G, Pickenäcker K, Pickenäcker O, Trimis D, Wawrzinek K, Weber T. Numerical and experimental investigation of matrix-stabilized methane/air combustion in porous inert media. *Combust. Flame* **2000**, *123*, 201–213. DOI:10.1016/s0010-2180(00)00163-2
87. Costa Oliveira FA, Dias S, Vaz MF. Behaviour of open-cell cordierite foams under compression. *J. Eur. Ceram. Soc.* **2006**, *26*, 179–186. DOI:10.1016/j.jeurceramsoc.2004.10.008
88. Zheng H, Zheng X, Chen Y. The Influence of Foam Ceramic Cell Structure on Methane Combustion Characteristics. *Ind. Furnace* **2023**, *45*, 5–11. DOI:10.3969/j.issn.1001-6988.2023.05.002
89. Zhang M, An Z, Wang L, Wei X, Jianayihan B, Wang J, et al. The regulation effect of methane and hydrogen on the emission characteristics of ammonia/air combustion in a model combustor. *Int. J. Hydrogen Energy* **2021**, *46*, 21013–21025. DOI:10.1016/j.ijhydene.2021.03.210
90. Yin X, Cheng L, Zhang L. Oxidation behaviors of C/SiC in the oxidizing environments containing water vapor. *Mater. Sci. Eng. A* **2003**, *348*, 47–53. DOI:10.1016/s0921-5093(02)00644-5
91. Ridley M, Garcia E, Kane KSSPB. Environmental barrier coatings on enhanced roughness SiC: Effect of plasma spraying conditions on properties and performance. *J. Eur. Ceram. Soc.* **2023**, *43*, 6473–6481. DOI:10.1016/j.jeurceramsoc.2023.06.049
92. Lee KN, Fox DS, Bansal NP. Rare earth silicate environmental barrier coatings for SiC/SiC composites and Si_3N_4 ceramics. *J. Eur. Ceram. Soc.* **2005**, *25*, 1705–1715. DOI:10.1016/j.jeurceramsoc.2004.12.013
93. Seo HI, Kim D, Lee KS. Crack Healing in Mullite-Based EBC during Thermal Shock Cycle. *Coatings* **2019**, *9*, 585. DOI:10.3390/coatings9090585
94. Ridley M, Opila E. Variable thermochemical stability of $RE_2Si_2O_7$ (RE = Sc, Nd, Er, Yb, or Lu) in high-temperature high-velocity steam. *J. Am. Ceram. Soc.* **2022**, *105*, 1330–1342. DOI:10.1111/jace.18120
95. Paglia L, Pedrizzetti G, Bottacchiari R, Bartuli C, Marra F, Pulci G. Scandium and Yttrium/Ytterbium Disilicates as Environmental Barrier Coatings: Microstructural Characterization and High-Temperature Water Vapor Exposure Tests. *J. Therm. Spray Technol.* **2026**, *35*, 101–121. DOI:10.1007/s11666-025-02115-z
96. Yu Y, Cai X, Cao Z, Jiao X, Xie W, Yu Y, et al. Effect of the heating rate on the thermal explosion behavior and oxidation resistance of 3D-structure porous NiAl intermetallic. *Mater. Charact.* **2022**, *190*, 112062. DOI:10.1016/j.matchar.2022.112062
97. Su SS, Lai WH, Hwang SJ. An Experimental Investigation of a Mini-Scale Porous Mmedia Combustor for Hydrogen Combustion. *J. Chin. Soc. Mech. Eng. Ser. C* **2017**, *38*, 373–380. Available online: https://www.airitilibrary.com/Article/Detail/02579731-201708-201710250007-201710250007-373-380 (accessed on 30 July 2026).
98. Song F, Wen Z, Fang Y, Wang E, Liu X. Combustion Wave Propagation of a Modular Porous Burner with Annular Heat Recirculation. *J. Therm. Sci.* **2020**, *29*, 98–107. DOI:10.1007/s11630-019-1162-0
99. Ballatore A, Somers LMT, van Oijen JA. A parametric study of high-pressure direct injections of hydrogen in an argon–oxygen environment by using large-eddy simulation and tabulated chemistry. *Fuel* **2025**, *397*, 135440. DOI:10.1016/j.fuel.2025.135440
100. Chen D, Chen J, Huang A, Fu L, Gu H. Preparation and water vapor corrosion behavior of AlN polytype bonded SiC bricks. *J. Alloys Compd.* **2022**, *918*, 165727. DOI:10.1016/j.jallcom.2022.165727
101. Yu M, Sun R, Luo G, Wang L, Li X, Yao H. Ammonia partial cracking over low-cost Ni catalysts for enhancing combustion. *Fuel* **2024**, *367*, 131306. DOI:10.1016/j.fuel.2024.131306
102. Civera A, Pavese M, Saracco G, Specchia V. Combustion synthesis of perovskite-type catalysts for natural gas combustion. *Catal. Today* **2003**, *83*, 199–211. DOI:10.1016/s0920-5861(03)00220-7
103. Zhang H, Zhou J, Du J, Yu Z, Liang X, Cheng YB, et al. Ammonia-methane flames stabilized in an ordered porous media burner. *Energy Fuels* **2025**, *39*, 6654–6670. DOI:10.1021/acs.energyfuels.5c00767

104. Qu H, Gou X. NOx emission characteristics of ammonia–hydrogen–air premixed swirl combustion in two-stage rich-lean combustor. *J. Combust. Sci. Technol.* **2024**, *30*, 32–42. DOI:10.11715/rskxjs.R202312011
105. Valera-Medina A, Pugh DG, Marsh P, Bulat G, Bowen P. Preliminary study on lean premixed combustion of ammonia-hydrogen for swirling gas turbine combustors. *Int. J. Hydrogen Energy* **2017**, *42*, 24495–24503. DOI:10.1016/j.ijhydene.2017.08.028
106. Hayakawa A, Goto T, Mimoto R, Kudo T, Kobayashi H. NO formation/reduction mechanisms of ammonia/air premixed flames at various equivalence ratios and pressures. *Mech. Eng. J.* **2015**, *2*, 14–00402. DOI:10.1299/mej.14-00402
107. Prisco LP, Ponton PI, Guaman MV, Avillez RR, Romao CP, Johnson MB, et al. Assessment of the Thermal Shock Resistance Figures of Merit of $Al_2W_3O_{12}$, a Low Thermal Expansion Ceramic. *J. Am. Ceram. Soc.* **2016**, *99*, 1742–1748. DOI:10.1111/jace.14160
108. Zhao XJ, Ru HQ, Chen DL, Zhang N, Liang B. Thermal shock behavior of nano-sized SiC particulate reinforced AlON composites. *Mater. Sci. Eng. B* **2012**, *177*, 402–410. DOI:10.1016/j.mseb.2012.01.019
109. Liu Y, Li C, Feng S, Wang Y, Zhou S, Jin S. Research Progress on Failure Mechanism, Material Selection and Structural Design of Long-Life Thermal Barrier Coatings. *China Surf. Eng.* **2024**, *37*, 220–237. DOI:10.11933/j.issn.1007-9289.20231008002
110. Fitzgerald K, Shepherd D. Review of SiCf/SiCm corrosion, erosion and erosion-corrosion in high temperature helium relevant to GFR conditions. *J. Nucl. Mater.* **2018**, *498*, 476–494. DOI:10.1016/j.jnucmat.2017.09.010
111. *ASTM C1525-2004(2009)*; Standard Test Method for Determining the Thermal Shock Resistance of Advanced Ceramics by Water Quenching Technique. ASTM International, West Conshohocken, PA, USA, 2009.
112. Zhang C, Yang B, Luo HK. Deep learning driven uncertainty quantification analysis for combustion modeling of turbulent non-premixed jet flames. *Appl. Energy Combust. Sci.* **2026**, *26*, 100491. DOI:10.1016/j.jaecs.2026.100491
113. Aayan B. Integrated Multiscale Modeling of Solid Oxide Electrodes, Cells, Stacks, and Systems. *Chem. Ing. Tech.* **2022**, *94*, 766–773. DOI:10.1002/cite.202100199